Journal of Geriatric Cardiology | JGC
REVIEW
J Geriatr Cardiol 2024; 21(5): 550–576

Cardiovascular computed tomography in cardiovascular disease: An overview of its applications from diagnosis to prediction

Zhong-Hua SUN[1,2,✉]

1. Discipline of Medical Radiation Science, Curtin Medical School, Curtin University, Perth, Australia; 2. Curtin Health Innovation Research Institute (CHIRI), Curtin University, Perth 6012, Australia
✉ Correspondence to: z.sun@curtin.edu.au
https://doi.org/10.26599/1671-5411.2024.05.002

ABSTRACT Cardiovascular computed tomography angiography (CTA) is a widely used imaging modality in the diagnosis of cardiovascular disease. Advancements in CT imaging technology have further advanced its applications from high diagnostic value to minimising radiation exposure to patients. In addition to the standard application of assessing vascular lumen changes, CTA-derived applications including 3D printed personalised models, 3D visualisations such as virtual endoscopy, virtual reality, augmented reality and mixed reality, as well as CT-derived hemodynamic flow analysis and fractional flow reserve (FFRCT) greatly enhance the diagnostic performance of CTA in cardiovascular disease. The widespread application of artificial intelligence in medicine also significantly contributes to the clinical value of CTA in cardiovascular disease. Clinical value of CTA has extended from the initial diagnosis to identification of vulnerable lesions, and prediction of disease extent, hence improving patient care and management. In this review article, as an active researcher in cardiovascular imaging for more than 20 years, I will provide an overview of cardiovascular CTA in cardiovascular disease. It is expected that this review will provide readers with an update of CTA applications, from the initial lumen assessment to recent developments utilising latest novel imaging and visualisation technologies. It will serve as a useful resource for researchers and clinicians to judiciously use the cardiovascular CT in clinical practice.

Computed tomography (CT) is a widely used imaging modality in the clinical practice, owing to its widespread availability and high diagnostic value. Over the last decades, CT has undergone rapid developments from the standard use of 64-slice CT to even fast scanners with improved spatial and temporal resolution, and from single energy to dual energy models.[1-35] More recently, the emergence of photon-counting CT represents the latest development in CT technology.[36-38] In routine clinical practice, CT images in 2D axial, multiplanar reformation, and 3D visualisations are commonly used to provide diagnostic information such as assessment of degree of lumen stenosis in cardiovascular system, identification and analysis of lesions such as atherosclerotic plaques in the vascular wall, as well as assessment of disease extent. This meets most of the clinical requirements for diagnostic purpose. However, standard cardiovascular CT angiography (CTA) may not allow for comprehensive assessment of the complexity of the lesions due to its limited role in providing functional assessment of cardiovascular disease. The integration of advanced technologies such as 3D visualisations and CT-derived applications into cardiovascular CT has transformed the diagnosis and treatment of cardiovascular disease.[39,40] These technologies include 3D visualisations such as virtual intravascular endoscopy, virtual reality (VR), augmented reality (AR) and mixed reality (MR), 3D printed patient-specific models using CT data, CT-derived fractional flow reserve (FFRCT) and hemodynamic analysis, and the increasing use of artificial intelligence (AI), machine learning (ML) and deep learning (DL) tools in cardiovascular disease.[41-50]

In this review article, I will first provide a brief summary of CT technological developments, followed by detailed overview of cardiovascular CT applications with use of these advanced technologies based on my research experience in cardiovascular CT imaging. It is expected that this article serves as a useful resource for readers or research-

ers to be aware of the spectrum of cardiovascular CT applications including the latest developments in this field, and how the judicious use of cardiovascular CT will revolutionise the current practice by enhancing diagnostic accuracy, facilitating surgical planning and optimising interventional or surgical approaches.

TECHNOLOGICAL DEVELOPMENTS IN CARDIOVASCULAR CT

Cardiovascular CT puts a strong demand on the technological advancements in imaging techniques mainly due to the fact that cardiac CT requires high spatial and temporal resolution to ensure acquisition of CT images with satisfactory quality, even during the rapid heartbeat. Cardiac CT drives the developments of CT technologies represented by the increasing use of CT scanners with fast gantry rotation speed, such as dual-source CT and dual-energy CT, which is widely available in many clinical sites. The most recent model of photon-counting CT (PCCT) received FDA approval in 2021 and increasing reports showed promising results of this latest technology in advancing CT applications.[36-38,51,52] In the area of cardiovascular CT, PCCT has significantly improved the diagnostic performance of CT in cardiovascular disease and other areas when compared to the standard CT. Table 1 is a summary of PCCT in cardiovascular applications, while Figures 1 and 2 are examples showing improved visualisation of calcified coronary plaques and stents with use of PCCT.[36,37]

3D VISUALISATIONS ENHANCING DIAGNOSTIC VALUE OF CARDIOVASCULAR CT

In addition to the standard 2D and 3D reconstructions, advanced 3D visualisations derived from cardiovascular CT have greatly enhanced the diagnostic value of CT in cardiovascular disease when compared to the standard approaches of lumen assessment. This is manifested in generating various 3D views which are detailed below with their corresponding clinical applications.

Virtual Intravascular Endoscopy (VIE) Providing Unique Intraluminal Views

Virtual endoscopy (VE) was introduced in early 90s with uniqueness of providing intraluminal views of the hollow organs and structures.[53-55] The most important and widely used application of VE is the virtual colonoscopy which allows for detection of colonic polyps less invasively when compared to the reference method of colonoscopy, thus serving as a screening tool. Virtual colonoscopy or CT colonography is a widely used technique for screening colorectal cancer with many reports proving its clinical value.[56-58] Virtual intravascular endoscopy (VIE) represents another application of VE to provide intraluminal visualisations of vascular structures,[41,59]

Table 1 Benefits of photon-counting detectors and impact on cardiovascular applications. Reprinted with permission under open access from Cademariti et al. [37]

Benefits of Photon-Counting Detectors	Potential Cardiovascular Applications
Higher spatial resolution	Stent imaging Coronary lumen evaluation Atherosclerotic plaque imaging Coronary artery calcium scoring Aortic valve calcification score
Improved iodine signal	Coronary lumen evaluation Stent imaging
Multi-energy acquisition	Coronary lumen evaluation Atherosclerotic plaque imaging Dose reduction Coronary artery calcium scoring Aortic valve calcification score
Energy binning	Stent imaging Atherosclerotic plaque imaging Dose reduction Myocardial tissue characterization.
Artifact reduction	Coronary lumen evaluation Stent imaging Atherosclerotic plaque imaging

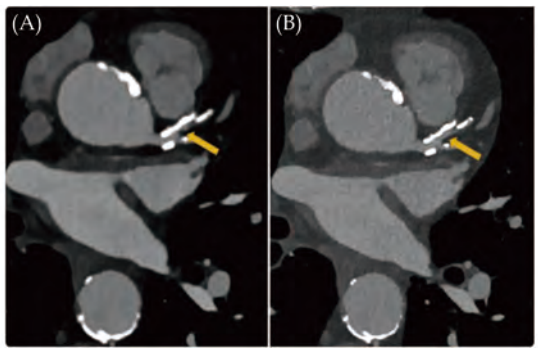

Figure 1 An 82-year-old man with coronary artery disease. Visualisation of calcified plaques and lumen diameter of the proximal left anterior descending was improved in the high resolution photon counting CT image ('B' with 0.2 mm slice thickness) when compared with the standard CT ('A' with 0.6 mm slice thickness). Arrow refers to the coronary lumen. Reprinted with permission under open access from Flohr, *et al*.[36]

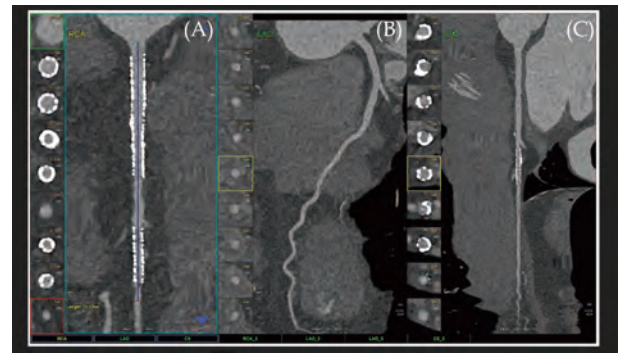

Figure 2 Cardiac PCCT visualisation of coronary stents and stented lumen. There are two stents at the level of the proximal and middle RCA (A) and one stent on the marginal branch of the left LCx (C); the LAD (B) is normal without any detectable atherosclerotic disease. All stents are perfectly visualised in their inner struts and also in their inner lumen, which is difficult to visualize on standard cardiac CT. Reprinted with permission under open access from Cademartiri, *et al*.[37] LAD: left anterior descending; LCx: left circumflex; PCCT: photon counting CT; RCA: right coronary artery.

such coronary artery lumen and ostium (Figure 3), plaques inside the coronary lumen (Figure 4), coronary stents (Figure 5),[60-64] aortic dissection (Figure 6) and aortic aneurysm (Figure 7),[65-67] and pulmonary embolism (Figures 8-10).[68] VIE has been shown to provide more accurate assessment of the lumen stenosis when compared to the standard use of 2D or 3D reconstructions, [69] present intraluminal views of aortic dissection, especially details of intimal tears and intimal flap of aortic dissection that are difficult to visualise on 2D views (Figure 11).[69,70] VIE also demonstrates the extent of thrombus involving arterial branches in pulmonary embolism.[68] Our previous studies and others have shown the usefulness of VIE in demonstrating suprarenal stent struts across the renal and other aortic ostium in patients with abdominal aortic aneurysm following treatment by endovascular aortic stent grafting (Figure 12).[70-86] In patients with calcified coronary plaques, VIE shows improved diagnostic value than that from coronary lumen assessment, hence con-

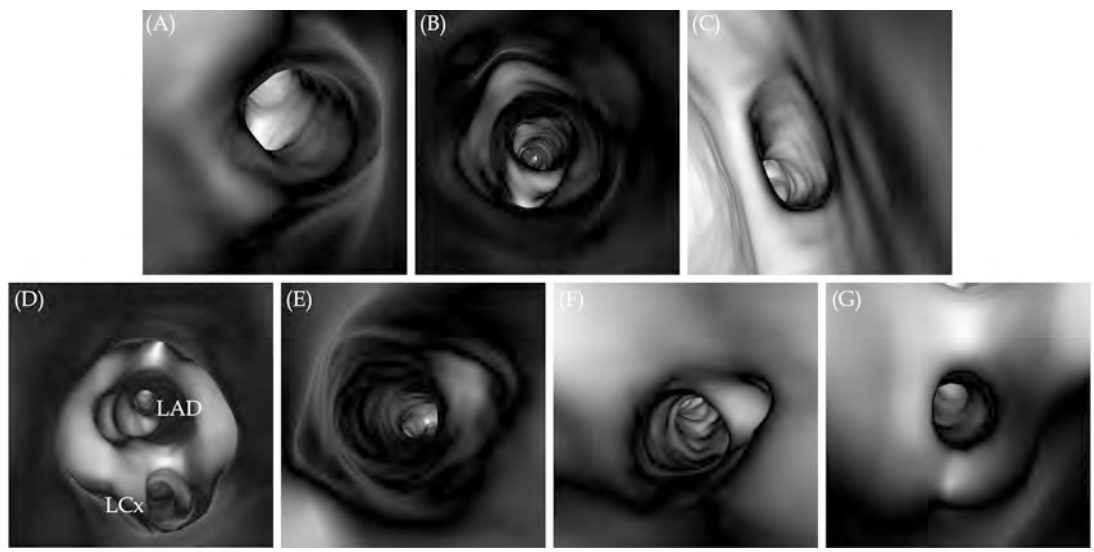

Figure 3 VIE views of normal coronary ostium. (A): Looking at the RCA ostium; (B): close view inside the RCA ostium; (C): looking at the left coronary ostium; (D): close view of LAD and LCx ostia; (E, F and G): inside views of LAD, LCx and ramus intermedius, respectively. LAD: left anterior descending; LCx: left circumflex; RCA: right coronary artery; VIE: virtual intravascular endoscopy.

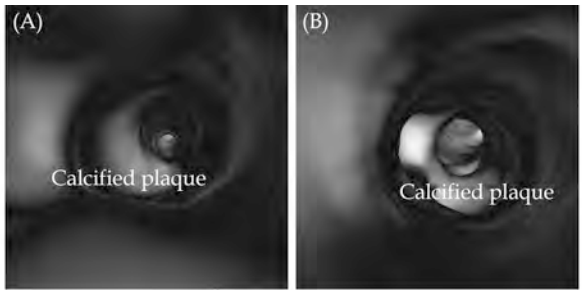

Figure 4 VIE visualisation of coronary plaques. (A): VIE view of calcified plaque at LAD; (B): VIE view of calcified plaque at RCA. These plaques present as a protruding sign in the coronary lumen without causing significant stenosis. LAD: left anterior descending; RCA: right coronary artery; VIE: Cvirtual intravascular endoscopy.

tributing to reducing unnecessary invasive procedures by improving specificity and positive predictive value (Figure 4).[60-64]

Coronary Bifurcation Angle Measurements Improving Diagnostic Value

One of the main limitations of cardiac CTA is lack of accurate assessment of calcified plaques due to blooming artifacts which significantly affect the specificity and positive predictive value.[87-90] Use of coronary bifurcation angle to determine the degree of coronary artery stenosis is a novel approach to overcome the limitation of lumen-based assessment with results proving its improved clinical value.[91-101] Our research group and others have shown that use of left coronary bifurcation angle to measure the angulation between left anterior descending (LAD) and left circumflex (LCx) arteries is more accurate in the assessment of calcified plaques when compared to the standard lumen assessment.[92,94,99,101] It is generally agreed that the wider angulation at the

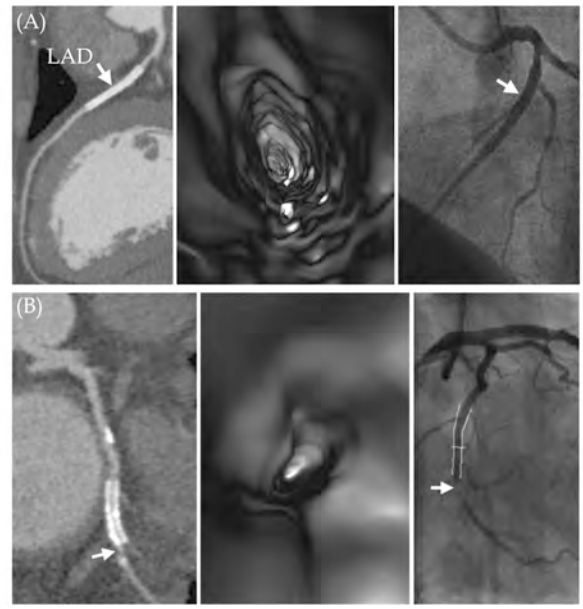

Figure 5 VIE visualisation of coronary stents in comparison with CCTA and ICA. (A): A case of true negative results for both CCTA and VIE. A 45-year-old female with hypertension and type 2 diabetes mellitus and has a metallic stent (arrow) placed in the left anterior descending artery. Both CCTA and VIE (left and middle images) showed patency of the stent without in-stent restenosis, and this was confirmed by ICA (arrow) (right image). (B): Another case of true positive result for both CCTA and VIE. A 57-year-old man with hypertension and obesity and with a total calcium score of 1125. A metallic stent was placed in the left circumflex artery. Both CCTA and VIE (left and middle images) showed in-stent restenosis at the distal edge of the stent (arrow). This was confirmed by ICA with 88% stenosis (arrow in right image). Reprinted with permission under open access from Wu *et al*.[64] CCTA: coronary computed tomography angiography; ICA: invasive coronary angiography; VIE: virtual intravascular endoscopy.

left coronary artery, the higher risk of developing coronary artery disease (CAD) as validated by our and other studies. Figure 13A is an example of a patient without having CAD, with measured LAD-LCx be-

Figure 6 VIE views of aortic dissection. (A): An intimal flap separates the aortic intimal layer into true lumen and false lumen; (B): VIE view inside the true lumen to demonstrate the three main branches arising from the aortic arch, namely, left subclavian artery, left common carotid artery and brachiocephalic artery; (C): inside view of the false lumen. VIE: virtual intravascular endoscopy.

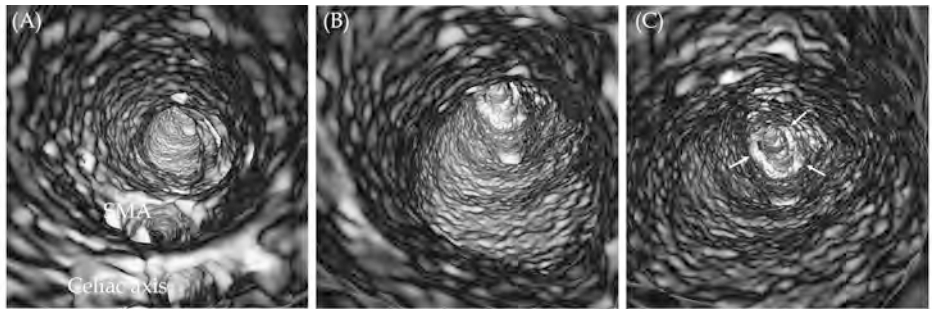

Figure 7 VIE view of an infrarenal abdominal aortic aneurysm. (A): VIE looking towards the aneurysm with celiac axis and SMA ostia; (B): inside view of the aortic aneurysm, and (C) with VIE view further down to the aneurysm towards common iliac arteries (arrows). Note that the intraluminal views of aortic wall, especially inside the aneurysm is irregular, most likely due to dilated aneurysm with thrombus formation which causes irregular wall changes. SMA: superior mesenteric artery; VIE: virtual intravascular endoscopy.

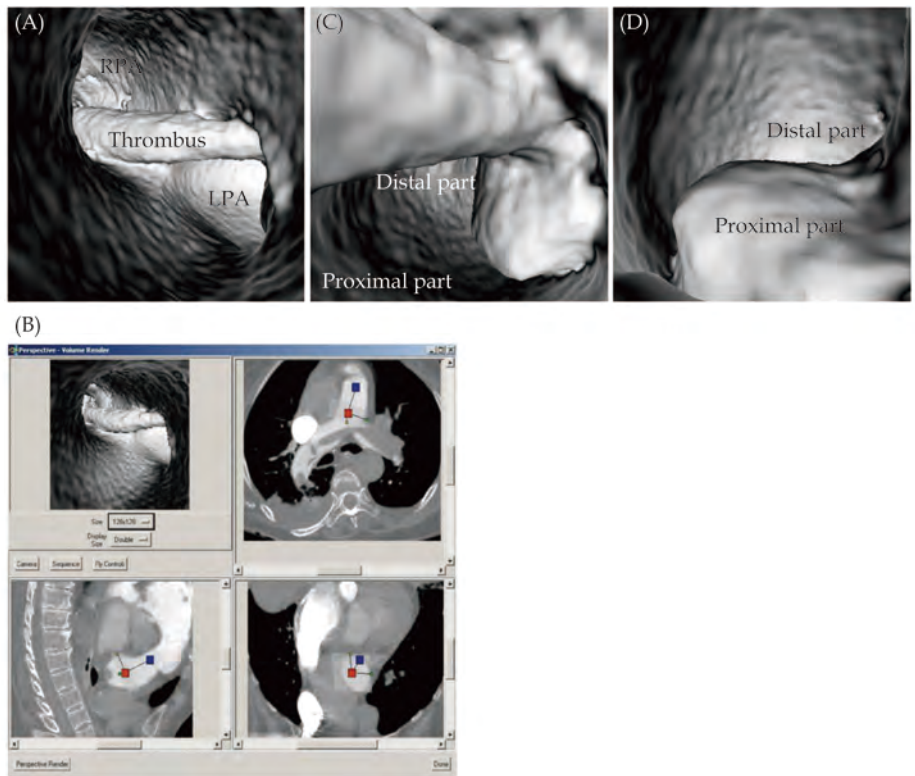

Figure 8 Pulmonary embolism involving bilateral pulmonary artery branches. (A): Large thrombus is present in left main pulmonary artery and it extends to right side; (B): orthogonal views show that viewing position is located in pulmonary trunk; (C & D): continuous extension of thrombus from proximal part of main pulmonary artery to distal segment with lumen narrowing, as well as protruding sign in lumen. LPA: left pulmonary artery. Reprinted with permission under open access from Sun, *et al.*[68]

ing 82.2°, while Figure 13B is another example of a patient with multiple calcified plaques at LAD causing significant stenosis, and the measured LAD-LCx angle is 105.9°.

Very little research is done at investigating the relationship between right coronary artery (RCA) angle and the CAD as most of the current studies focus on the left coronary artery bifurcation where usually atherosclerosis forms. We have pioneered some preliminary research on investigating the correlation between RCA and aorta and our results proved the association of RCA-aorta angle with CAD.[102,103] Our recent research through analysis of 250 patients revealed that that a smaller RCA-aorta angle was associated with CAD development when compared to the normal group (79.07° ± 24.88° *vs.*

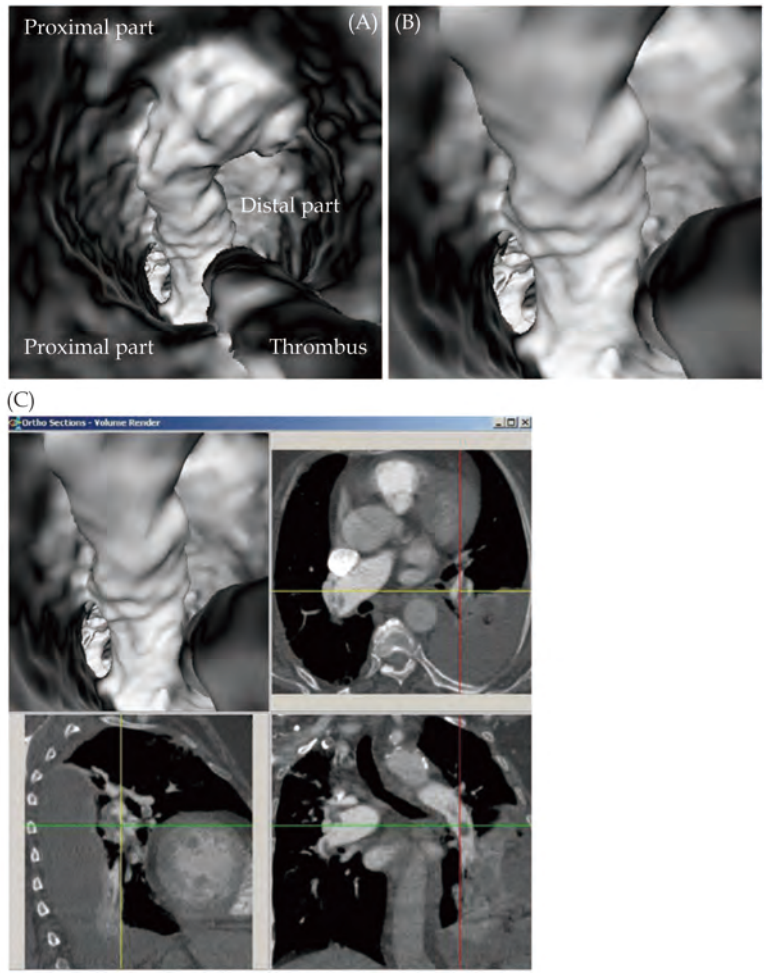

Figure 9 Virtual intravascular endoscopy views of left lower lobar embolism from proximal to distal segments of lobar artery. (A): VIE view of proximal segment of left lower lobar pulmonary artery with thrombus; (B): VIE view of distal segment of left lower lobar pulmonary artery with thrombus; (C): Accurate position of thrombus is confirmed with using multiplanar views. VIE: virtual intravascular endoscopy. Reprinted with permission under open access from Sun, *et al.* [68]

92.08° ± 19.51°, P = 0.001), narrower angle in smokers than non-smokers 76.63° ± 22.94° *vs.* 85.25° ± 23.84°, P = 0.016). A narrow RCA-aorta angle was found to be negatively correlated with body mass index (r = −0.174, P = 0.010).[103] Figure 14 shows the RCA-aorta angles in two different patients. More studies from different population groups are needed to validate our findings.

VR/AR/MR Enhancing Standard Image Visualisations

Advancements of 3D visualisation technologies have enhanced the value of standard image visualisations in the diagnosis of cardiovascular disease, and these 3D innovative technologies including VR, AR and MR have shown great potential from medical education to surgical planning and simulation of complex or challenging procedures.[42,104-110] VR provides the user with an immersive 3D virtual environment usually through a head-mounted device, while AR enables the user to interact with virtual models. MR is an advancement of AR allowing the display of virtual objects on real world settings (Figures 15 and 16).[110]

Increasing studies show that VR and AR enhance student's learning of anatomy and pathology through displaying complex 3D anatomical structures.[42,111-113] These tools are playing an important role during the covid-19 pandemic which restricts the access to cadavers or specimens for medical education. Moro et al conducted a systematic review of VR and AR

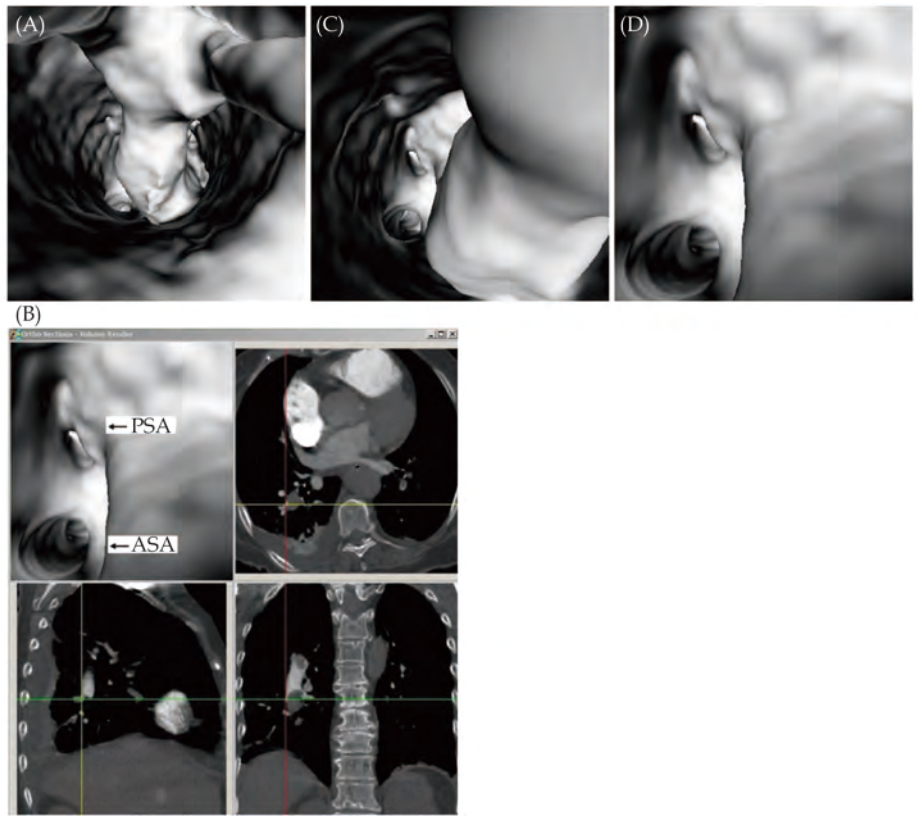

Figure 10 Virtual intravascular endoscopy views of right posterobasal segmental embolism. Thrombus extends from right lower lobar artery (A) to posterobasal segmental arteries (B and C). ASA: anteromedial basal segmental artery; PSA: posterobasal segmental artery. Reprinted with permission under open access from Sun, *et al.*[68]

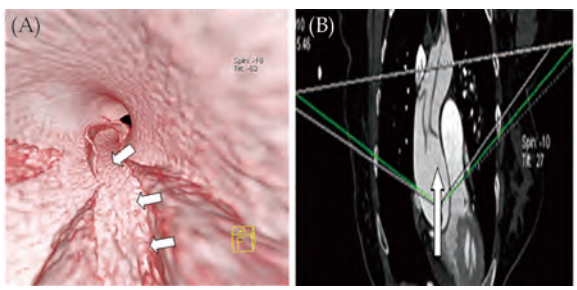

Figure 11 Irregular entry tear on VIE and MPR. (A): VIE shows a long irregular entry tear (arrow) on the intimal flap of a Stanford type A dissection viewed from the true lumen. (B): The MPR cannot show the actual configurations of the tear and flap. MPR: multiplanar reformation; VIE: virtual intravascular endoscopy. Reprinted with permission under open access from Qi, *et al.* [70]

in medical student's leaning anatomy and physiology through analysis of 8 studies.[114] When comparing VR (4 studies) and AR (5 studies) with traditional teaching methods, their analysis did not show significant differences in terms of knowledge scores (Figure 17). Barteit, *et al.*[42] analysed 27 studies about the value of VR, AR and MR in medical education. Participants in these studies included medical students and residents. These 3D visualisation tools were mainly used in surgery training (48%) and anatomy learning (15%) with analysis of findings showing positive impact on learning anatomy. These two review articles present evidence-based support to use VR and AR/MR as viable alternatives to the current teaching methods.

Recent studies from our research group compared the clinical value of VR and MR with 3D printed physical models and original CTA images in education and pre-surgical planning of congenital heart disease (CHD).[115,116] Due to variations of congenital heart anomaly, it is always challenging to understand the complex anatomy and pathology associated with CHD conditions. When compared to 3D printed models VR has been ranked as the preferred visualisation tool by healthcare professionals.[115] When comparing MR with 3D printed models in two selected CHD cases (one simple and one complex conditions), MR was found to be the

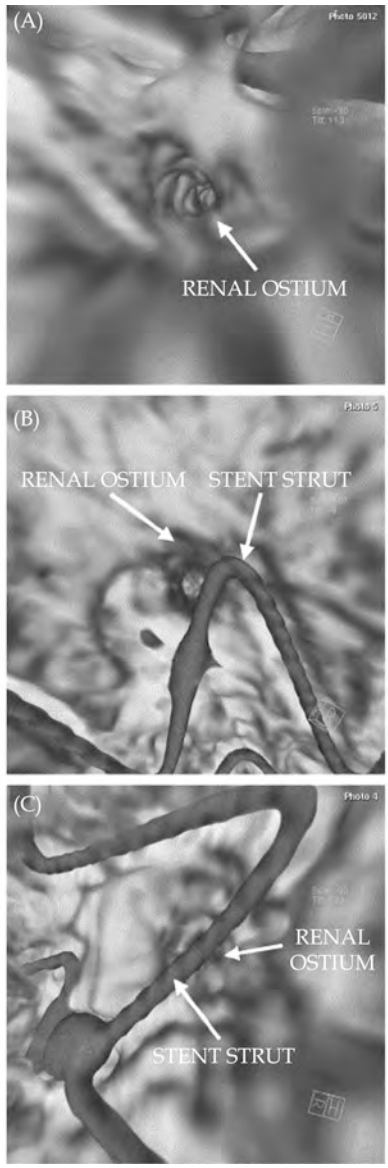

Figure 12 CT virtual intravascular endoscopic image. (A): A patient with no struts crossing the renal ostium; (B): CT virtual intravascular endoscopic image of a patient with a stent strut peripherally crossing the renal ostium; (C): CT virtual intravascular endoscopic image of a patient with a stent strut crossing the renal ostium in a central position. Reprinted with permission from England *et al.* [86]

best modality in demonstration of complex CHD lesions, enhancing learning cardiac pathology and depth perception, and facilitating preoperative planning (Figure 18), while 3D printed models were rated as the best tool for communication with patients.[116]

3D Printed Patient-specific Models Enhancing Diagnosis and Assisting Surgical Planning

3D printing has been used widely in the medical field with increasing evidence proving both educational and clinical value when compared to the traditional methods. Patient-specific or personalised models offer superior advantages over traditional

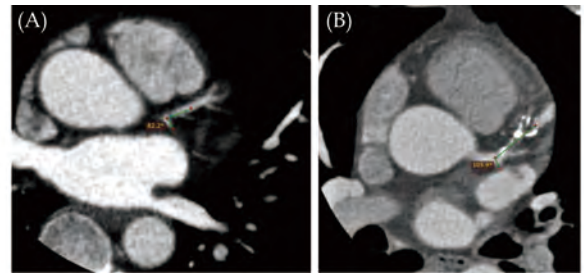

Figure 13 Correlation of LAD-LCx angle with CAD. (A): A narrow angle of 82.2° was measured between LAD and LCx coronary arteries on 2D axial image in a patient without CAD; (B): a wide angle of 105.9° was measured between LAD and LCx coronary arteries in a patient with multiple calcified plaques at the LAD resulting in significant stenosis. CAD: coronary artery disease; LAD: left anterior descending, LCx: left circumflex.

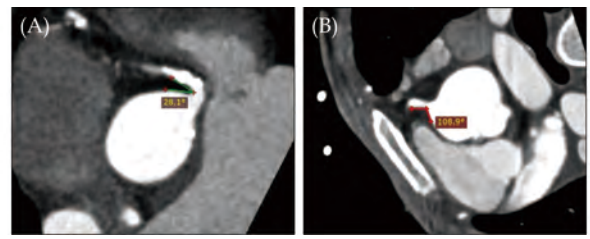

Figure 14 RCA-aorta angles in two different cases. (A): MPR images of a narrow (28.1°) RCA–aorta angle from an individual with CAD and calcified plaques. (B): A wide (108.9°) RCA–aorta angle from a normal case. CAD: coronary artery disease; MPR: multiplanar reformation; RCA: right coronary artery. Reprinted with permission under the open access from Geerlings-Batt, *et al.*[103]

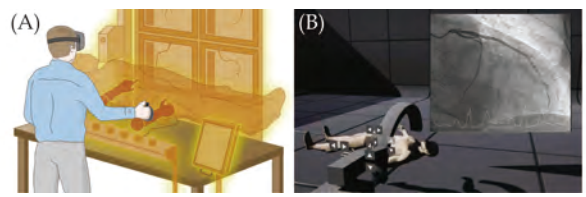

Figure 15 VR completely immersing the user in a virtual 3D space. (A): User is completely immersed in a virtual 3D space with use of a head-mounted display; (B): a real-life example of VR application allowing trainees to perform virtual coronary angiograms. VR: virtual reality. Reprinted with permission from Jun, *et al.*[110]

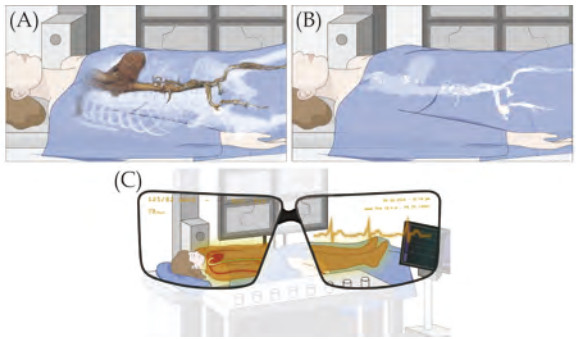

Figure 16 AR integrates superimposed virtual elements into a real-world environment. (A): 3D CT image of a patient's vasculature could be imaged by an operator; (B): vascular calcifications could be focused to guide the best puncture site and avoid complications during the procedure; (C): AR superimposes virtual elements into a real-world environment. AR: augmented reality. Reprinted with permission from Jun, *et al*.[110]

image visualisations as the physical models allow the user to have a direct visualisation of anatomy and pathology, in addition to having tactile experience. 3D printing technology has advanced rapidly over the last decades with capability of printing the models with flexible and multi-colour materials with high accuracy, even with the capability of 3D bioprinting organs and tissues.[117-130]

Use of 3D printed models in cardiovascular anatomy and pathology includes a range of applications from medical education to surgical planning and simulation of complex cardiovascular procedures, facilitating doctor-patient communication, and studying optimal CT scanning protocols for minimising radiation exposure.[131-160] Studies have proved that 3D printed heart and vascular models significantly increased students' knowledge and understanding of cardiovascular anatomy and pathology when compared to the current teaching tools (using cadavers, lectures or diagrams).[161-166] Figure 19 shows 3D printed heart and vascular models with multi-colour in comparison with the cardiac specimens, while Figure 20 is another example of 3D printed heart valve through using high-resolution micro-CT scanner with 0.1mm resolution.[167,168]

3D printed patient-specific models are also playing an important role in pre-surgical planning and simulation of cardiovascular procedures, and studies conducted at single and multi-centre sites confirmed the clinical value of 3D printed models. [164,169-175] Majority of these reports focus on the application of 3D printed models in assisting with CHD surgeries. When compared to the current surgical approaches based on 2D/3D image visualisations, surgical decision was changed or modified in up to 50% of cases with use of 3D printed models as part of the surgical planning (Figure 21). [130,170-172]

3D Printed Patient-specific Models Assisting Clinical Communication and Optimising CT Protocols

3D printed models also serve as a useful tool for improving communication between doctors and patients and within clinical colleagues.[169,176-178] The importance of using 3D printed physical models lies in its advantages of enhancing patients or parents of patients' understanding of disease condition and this is especially useful when dealing with complex or challenging scenarios where 3D printed models assist clinicians to better communicate with pa-

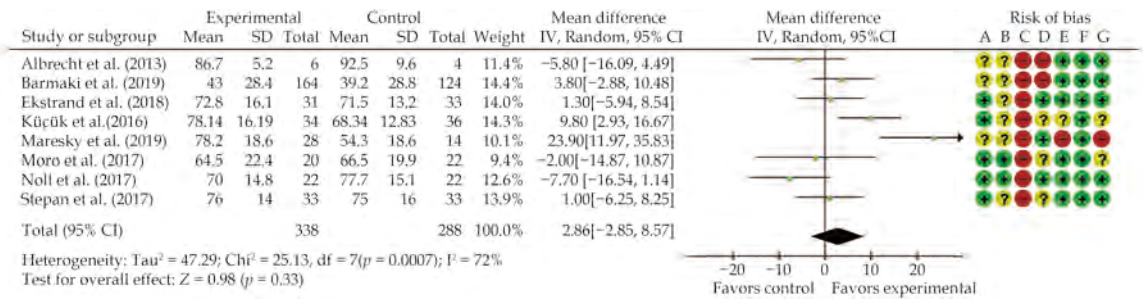

Figure 17 Mean difference between groups in knowledge scores (using percentages). (A): Random sequence generation (selection bias); (B): allocation concealment (selection bias); (C): blinding of participants and personnel (performance bias); (D): blinding of outcome assessment (detection bias); (E): incomplete outcome data (attrition bias); (F): selective reporting (reporting bias); and (G): other bias. Green colour indicates low risk of bias; yellow indicates unclear risk of bias; and red colour indicates high risk of bias. Reprinted with permission from Moro, *et al*.[114] "Control" indicates traditional teaching methods approaches; "Experimental" indicates augmented or virtual reality approaches.

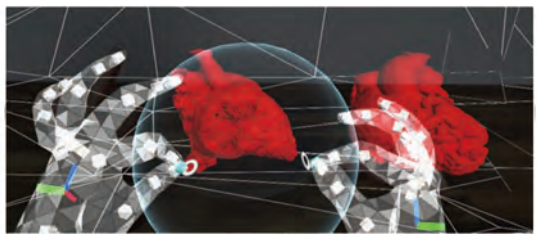

Figure 18 A screenshot using the HoloLens 2. The user is using the sphere to cut through the heart models in order to view the intra-cardiac structures. The sphere can be enlarged or sized down to change the amount of anatomy to be cut out. Reprinted with permission under open access from Lau *et al*.[116]

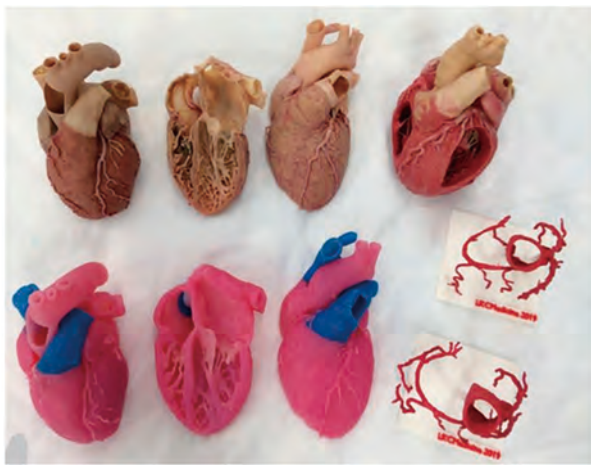

Figure 19 Learning materials provided to the study groups: phase 1 materials include plastinated cardiac specimens (top row) and their 3D printed replicas and the coronary vessels (bottom row). Reprinted with permission from Mogali *et al*. [167]

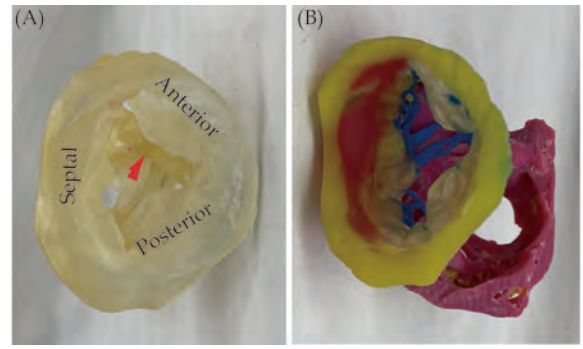

Figure 20 A 3D-printed model of the tricuspid valve of a human heart specimen (HH 223). (A): A model printed using a clear material as viewed from the atrium, with leaflets labeled and the moderator band marked with a red arrow; (B): a model printed using multiple colors and materials and rotated to show the subvalvular apparatus. Yellow, tricuspid annulus; transparent, mitral leaflets; blue, chordae tendinea; pink, papillary muscles. Reprinted with permission from Arango *et al*.[168]

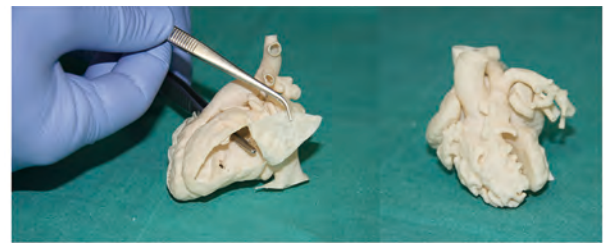

Figure 21 Surgical and interventional planning on 3D-printed heart models. DORV case, internal vision from the left ventricle (left). DORV (another case), external view (right). DORV-double outlet right ventricle. Reprinted with permission under the open access from Gomez-Ciriza *et al*.[130]

tients. Figure 22 shows that 3D printed models enhance communication with patients and colleagues based on a recent review.[169]

Use of 3D printed models to optimise CT scanning protocols is another new research area showing great promise, although only a few studies are available in the literature. [152-160] Our research group and others have developed heart and vascular models to study cardiovascular CT protocols with the aim of minimising radiation exposure without compromising image quality.[152-158] In particular, we have developed a type B aortic dissection model with simulation of endovascular stent grafting procedure for investigation of CTA protocols (Figures 23 and 24).[151,152] Another example of 3D printing application in this area is our developed 3D printed coronary artery models with simulation of calcified plaques to determine the optimal protocols for visualisation of coronary lumen due to presence of extensive calcification.[153] Figure 25 shows the 3D printed coronary models with various diameters and lengths of calcified plaques inserted into the main coronary arteries for studying optimal coronary CTA protocols. These early research lays foundation to further develop more realistic 3D printed models with inclusion of anatomical structures such as skin, muscle layers and other organs surrounding the heart and vascular structures.

CARDIOVASCULAR CTA-DERIVED FLOW DYNAMICS IN CARDIOVASCULAR DISEASE

Computational fluid dynamics (CFD) emerges as a rapidly developing tool in biomedical engineering research with capability of investigating hemodynamic changes in the cardiovascular system. Blo-

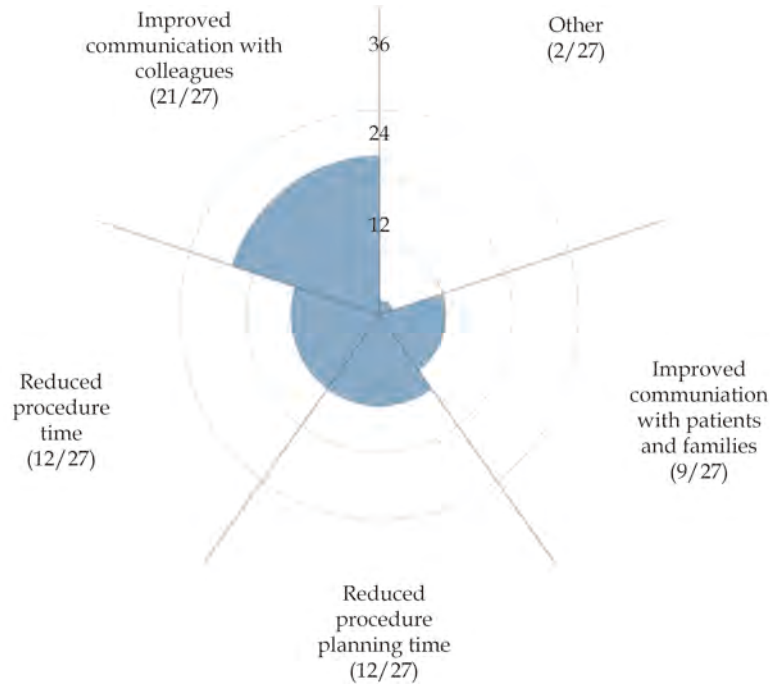

Figure 22 Participants' responses on how 3D-printed cardiac models improve communication with colleagues and patients/families. Reprinted with permission under open access from Illmann, *et al.*[169]

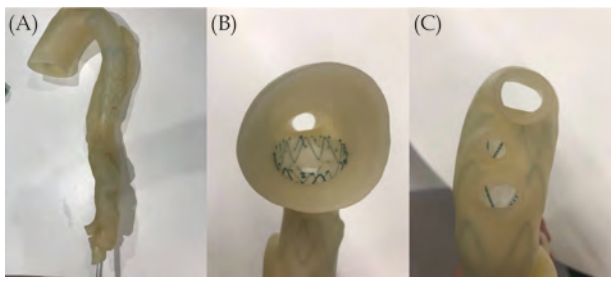

Figure 23 Stent graft deployed in a 3D-printed model. (A): Deployed stent graft visible through model wall; (B): axial view from proximal arch; (C): caudal view down arch vessels. Reprinted with permission under open access from Wu, *et al.* [152]

od flow plays an important role in the initiation and development of atherosclerosis because inflammatory change usually occurs in the anatomical area where blood flow is non-uniform and disturbed, thus affecting the behaviour of endothelial cells. CFD simulations allow calculation of hemodynamic changes such as flow velocity, wall pressure and wall shear stress within the vascular structures, hence providing further information about biomechanics of atherosclerosis and other cardiovascular disease which cannot be acquired from the standard imaging analysis.[179-202] Further, CFD allows for detection of high-risk plaques and plaque progression which contributes to improving patient care and reducing major adverse cardiac events.[198-200,203-205]

Since CFD simulations are based on geometric reconstruction of anatomical structures, most of the applications are derived from CT angiographic images. One of the pioneering applications performed in our research group is about investigation of CTA-derived CFD analysis of coronary plaques in relation to the left coronary bifurcation angles.[180,181,188,190,198-200] CFD simulations using CTA-generated realistic models confirmed findings as observed on coronary CTA images by identifying hemodynamic changes in the bifurcation region. Our analysis showed that wall shear stress was significantly increased in the bifurcation areas with angulation > 80° as opposed to little or no change in the narrow angulation models (< 80°). Flow velocity was increased at the post-stenotic regions as shown in Figures 26 and 27.

Another CFD application lies in the hemodynamic analysis of type B aortic dissection (TBAD) which draws increasing attention of research in recent years.[191-197,201] TBAD is a critical disease involving a tear in the descending aorta which allows blood to flow between the wall layers and results in a true lumen and false lumen. To understand blood flow characteristics in patients with TBAD, CFD simulations, in particular CFD derived from 2D- and 4D-

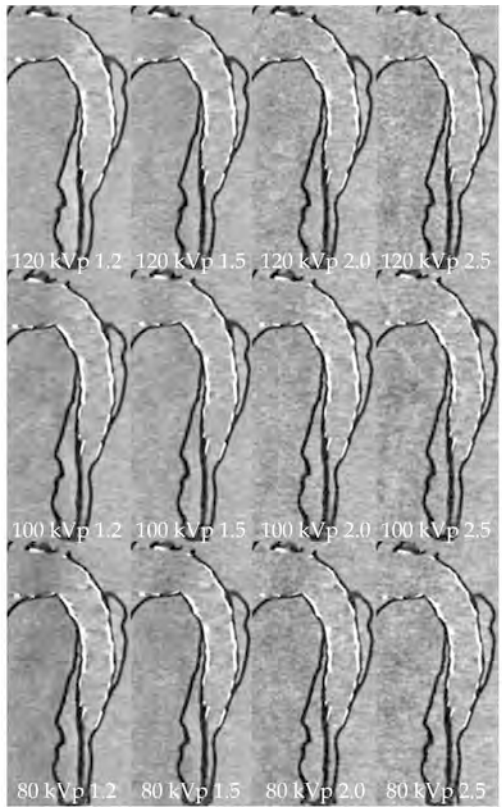

Figure 24 Sagittal reformatted images of CTA protocols. When kVp was decreased to 80, image noise increased with the use of high-pitch protocol values of 2.0 and 2.5. CTA: computed tomography angiography; kVp: kilovoltage peak. Reprinted with permission under open access from Wu, *et al*.[152]

flow MRI have been shown to accurately predict dissection hemodynamics, and its relationship with disease progression, such as false lumen thrombosis, false lumen growth etc which contribute to guiding patient management and enhancing outcomes through development of compliance-matching stent grafts.[194-197] Figures 28 and 29 are examples of CFD simulations based on CT angiographic images of hemodynamic changes in TBAD.[191]

Although coronary CTA is a widely used modality for the diagnostic assessment of coronary artery disease, it does not provide functional significance in relation to the degree of coronary stenosis. It is well known that the degree of coronary stenosis does not always correlate with the hemodynamic significance. Fractional flow reserve (FFR) is an established reference method for determining lesion-specific ischemia and serves as a valuable tool to guide patient treatment.[206-208] However, FFR is an invasive procedure requiring measurements of coronary pressure via pressure guidewire during invasive coronary angiography examinations. This has limited its widespread use in clinical practice. Coronary CTA-derived fractional flow reserve (FFRCT) has been confirmed by many single centre studies and multi-site clinical trials to improve diagnostic accuracy in the diagnosis of CAD over the standard coronary CTA alone.[209-219]

The main advantage of FFRCT lies in its superiority of providing combined assessment of coronary stenosis and hemodynamic significance through analysis of hemodynamic changes to the coronary

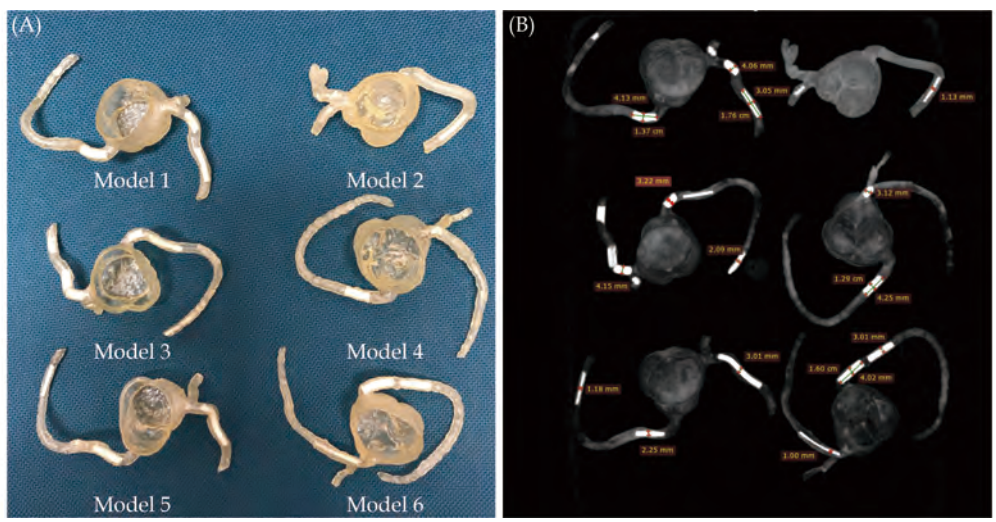

Figure 25 Three-dimensional printed patient-specific coronary models based on the simulation of calcified plaques in the coronary arteries. (A): Three-dimensional printed models (n = 6) with simulated calcified plaques in coronary artery branches; (B): measurements of plaque dimensions on 2D maximum-intensity projection images using 0.5 mm slice thickness. Reprinted with permission under open access from Sun, *et al*.[153]

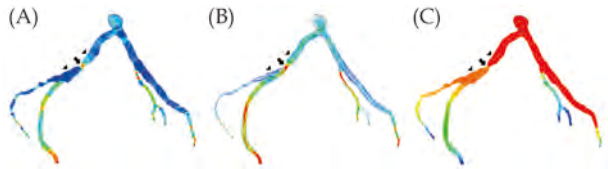

Figure 26 Correlation between wider angulation and hemodynamic changes by CCTA-derived CFD analysis. Left coronary bifurcation angle was measured 105° between the two main arterial branches, LAD and LCx with significant stenosis (> 70%) at LCx on CCTA and invasive coronary angiography in a 58-year-old man. (A and B): CFD analysis shows increased wall shear stress and flow velocity at the stenotic site of LCx. (C): CFD analysis shows decreased wall pressure at the same location. Arrow refers to the stenotic region at LCx, while arrowheads point to the pre- and post-stenotic locations. CCTA: coronary computed tomography angiography; CFD: computational fluid dynamic; LAD: left anterior descending; LCx: left circumflex. Reprinted with permission under the open access from Sun and Chaichana.[190]

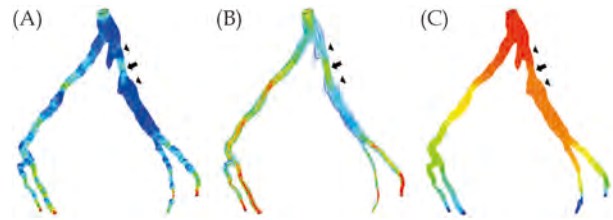

Figure 27 Correlation between narrower angulation and CCTA-derived CFD analysis. Left coronary bifurcation angle was measured 53° and 55.7° between LAD and LCx on CCTA and ICA in a 65-year-old male, respectively. Significant stenosis (> 60%) was noticed at LAD and LCx on CCTA, but no significant stenosis (42%-48%) was confirmed on ICA (images not shown). (A-C): No significant change was observed with wall shear stress, flow velocity and wall pressure. Arrow refers to the mild stenotic site of LAD, while arrowheads point to the pre- and post-stenotic locations. Reprint with permission under the open access from Sun and Chaichana.[190] CCTA: coronary computed tomography angiography; CFD: computational fluid dynamic; LAD: left anterior descending; LCx: left circumflex; ICA: invasive coronary angiography.

artery tree. This is especially manifested in the improved specificity in detecting hemodynamically significant CAD when compared to coronary CTA based on human observer assessment, thus leading to reduction of unnecessary invasive coronary angiography procedures.[209-215] Figure 30 is an example showing the value of FFRCT to diagnose coronary stenosis with accuracy validated by invasive FFR.[209] CT perfusion-FFR (CTP-FFR) is another novel approach by combining CT perfusion with FFRCT to further enhance the diagnostic value of coronary CTA in CAD as shown in our recent study.[219] Through analysis of 93 patients with a total of 103 coronary vessels, results of our recent work showed that CTP-FFR achieved higher performance than coronary CTA or FFRCT or CTP in CAD (Figures 31 and 32), and CTP-FFR was less affected by calcification than the traditional coronary CTA. A combination of CTP-FFR + CTP + FFRCT achieved the

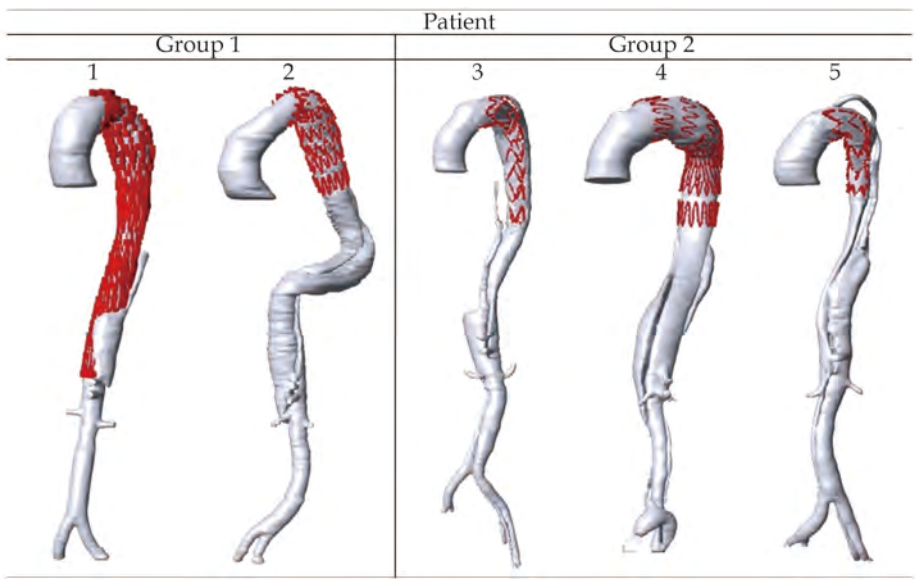

Figure 28 Three-dimensional reconstruction of complicated Stanford type B aortic dissection patients' geometry after SG repair. The red color showed the region of SG insertion. The SG will be used for illustration purpose only and will not be incorporated for simulation. Reprinted with permission from Wan Ab Naim *et al.*[191] SG: stent-graft.

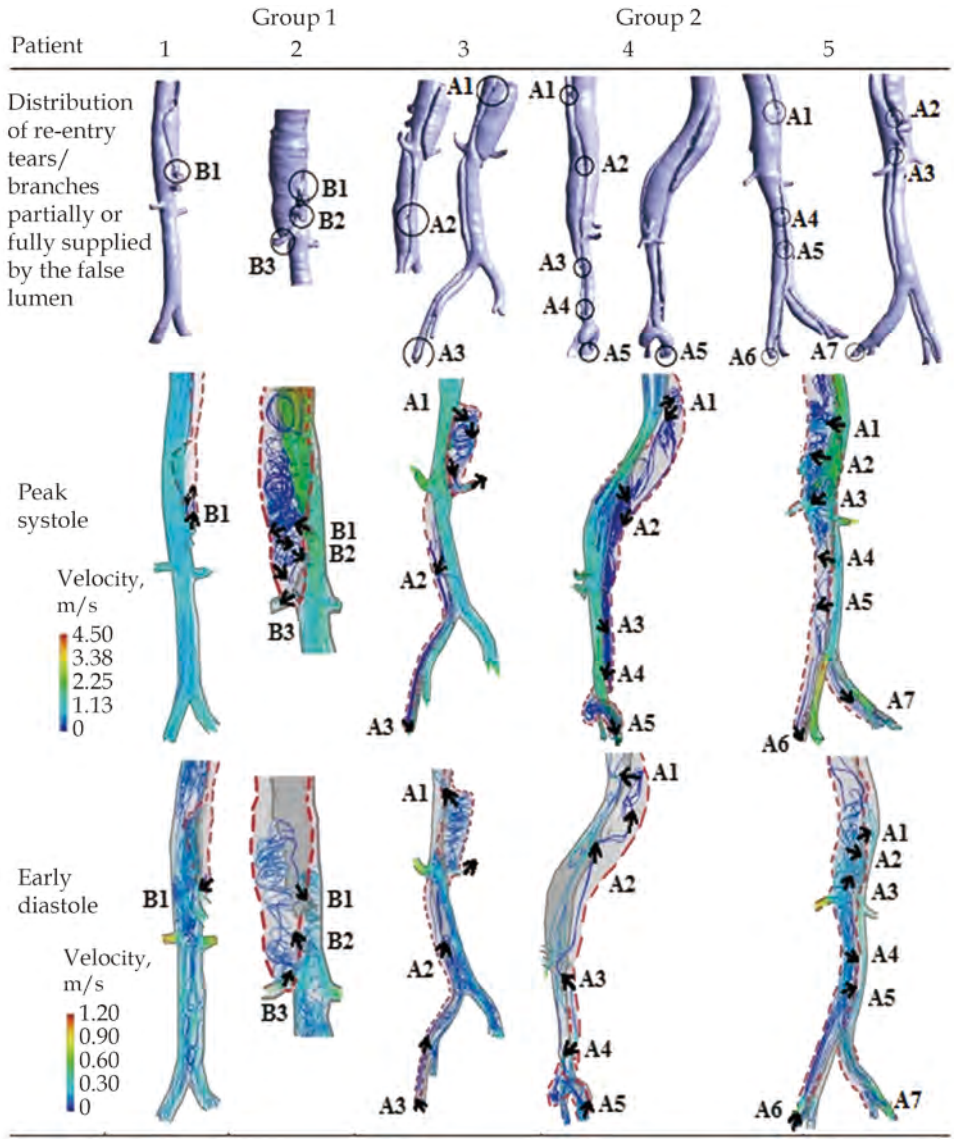

Figure 29 Blood flow pattern of 5 patients with CFD analysis of type B aortic dissection. The dashed red line is the FL. The black circles are locations of re-entry tears and abdominal branches partially supplied by the true lumen and FL. A1, re-entry tear 1; A2, re-entry tear 2; A3, re-entry tear 3; A4, re-entry tear 4; A5, re-entry tear 5; A6, re-entry tear 6; A7, re-entry tear 7. B1, branch 1; B2, branch 2; B3, branch 3 that are partially or fully supplied by FL. The results were obtained during peak systole and early diastole. FL: false lumen. Reprinted with permission from Wan Ab Naim *et al*.[191]

highest diagnostic value than that from these individual examinations.

With incorporation of DL models into FFRCT measurements, it is becoming more efficient to calculate hemodynamic changes from coronary CTA images, thus, FFRCT-guided patient management as a clinical decision-making tool is expected to become a first line modality in the near future.[220,221] Despite promising results available in the literature, some limitations will need to be overcome such as turnaround time of generating results, upfront costs and need to further improve specificity.[45]

AI APPLICATIONS IN CARDIOVASCULAR DISEASE

In recent years, medical AI has achieved significant progress in clinical specialties with AI tools showing considerable improvements in accuracy for clinical diagnosis and prediction of disease outcomes.[222-231] Applications of AI in cardiovascular disease are further enhanced with use of ML and

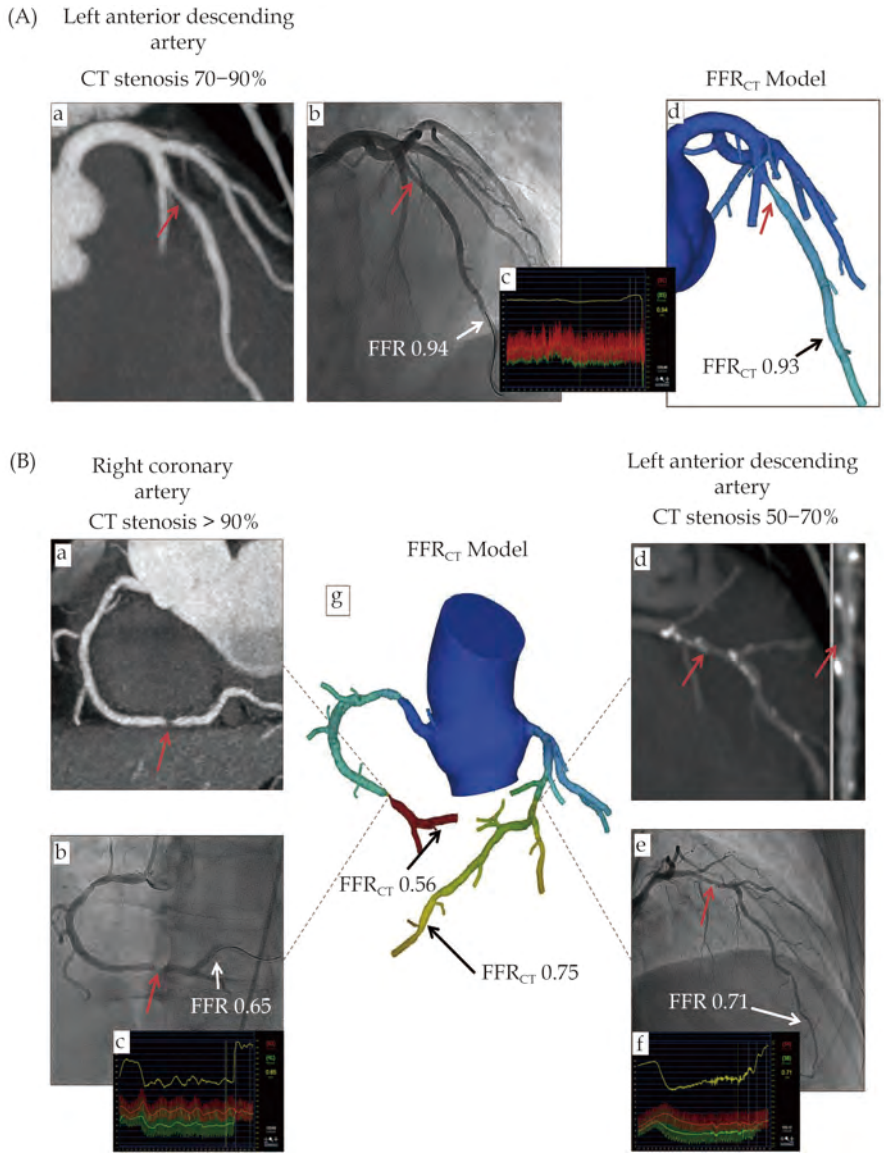

Figure 30 Examples of FFRCT in assessing the hemodynamic significance of coronary lesions at three main coronary arteries (A, B). Coronary CT angiography shows significant stenoses on the LAD, RCA, and LCx, while FFRCT shows ischemia at RCA and LCx but not at LAD, as the FFRCT value is more than 0.80. This was confirmed by invasive FFR measurements, as shown in (A(c)) and (B(c, f)). (a, b) in image (A), (a, b, d, e) in image (B) refer to stenotic lesions of RCA and LAD on coronary CT angiography and invasive FFR measurements, respectively, while ((A)d, (B)g) indicate FFRCT measurements at these coronary arteries. Reprinted with permission from Norgaard, et al.[209] FFRCT: fractional flow reserve derived from CT; LAD: left anterior descending artery; LCx: left circumflex; RCA: right coronary artery.

DL algorithms which enable analysis of patterns and relationships from imaging and non-imaging data to generate new insight into disease processes and develop new treatment therapies. There are many aspects of AI in cardiovascular disease with great potential to address issues such as timing, early detection and improved diagnostic accuracy, and accurate prediction of prognosis with better patient management.[222-226] ML and DL tools are applied to cardiac imaging modalities including echocardiography, coronary CT, cardiac MRI and cardiac nuclear medicine imaging to improve diagnosis, risk prediction and image interpretation.[48,49,232] In the following sections, I only highlight the applications of AI/ML/DL in CAD and other cardiovascular diseases from our experience, while readers are referred to some review articles on the comprehensive applications of AI in cardiovascular medi-

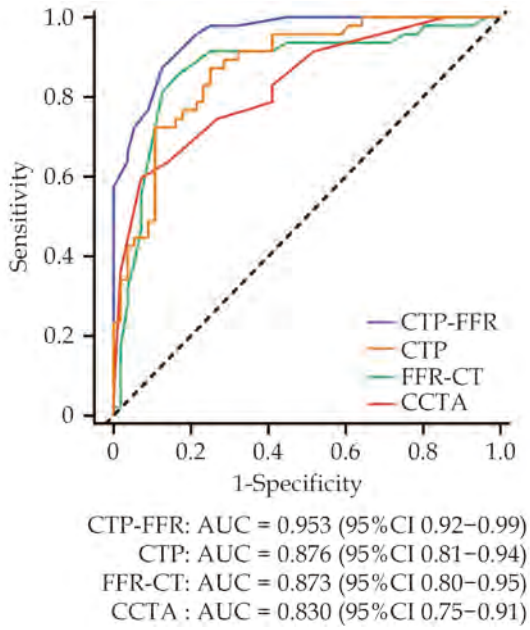

Figure 31 Graph showing diagnostic performance of CTP-FFR, CTP, FFR-CT and CCTA. AUC of receiver operating characteristics curve analysis is shown on per vessel for CTP-FFR, CTP, FFR-CT and visual stenosis grading (stenosis ≥ 50%) at CCTA. The dotted line represents the reference line. AUC: area under receiver operating characteristics curve; CCTA: coronary computed tomography angiography; CTP-FFR: computed tomography perfusion-derived fractional flow reserve. Reprinted with permission under open access from Go, *et al*.[219]

cine.[48,49,222,223]

ML/DL in Coronary Calcium and Coronary Artery Disease

Coronary calcium scoring (CAC) using coronary CT is a marker used to predict the risk of future cardiovascular events and it is commonly performed on non-contrast CT scans. The clinical value of CAC is well established, however, there are some obstacles that could limit its widespread applications in routine clinical practice. First, small clinical sites may not have resources (specialised software and technologists) to perform the task of coronary artery segmentation and quantification of calcium burden. Second, most of the patients undergoing routine chest CT scans for non-cardiac situations may have CAD detected but not routinely reported or quantified, thus missing the opportunity for early diagnosis or prevention.[233] Further, it is a time-consuming task to quantify CAC with involvement of human observers, thus automation of CAC scoring and coronary stenosis with use of AI tools has great potential to address these limitations.

Use of advanced DL models in cardiac CT image segmentation and analysis has shown high accuracy of automated quantification of calcium scores with excellent correlation with human observers (manual assessment) in terms of their diagnostic performance.[224,232,234-236] DL models have been validated on different datasets (from different CT scanners and ethnic groups) (Figure 33).[232] DL models also increase workflow of interpreting coronary CTA images by significantly reducing the time of image reconstructions and interpretation but with diagnostic value similar to expert observers.[223,224,232-236]

Another advantage of using DL in CAD is to improve the assessment of calcified plaques by increasing specificity and positive predictive value (PPV) when compared to the standard coronary CTA. [225,230,234,] Coronary CTA has low to moderate diagnostic value in CAD with heavily calcified plaques due to blooming artifacts associated with extensive calcification in the coronary artery which leads to high false positive rate. [86-90] Despite differ-

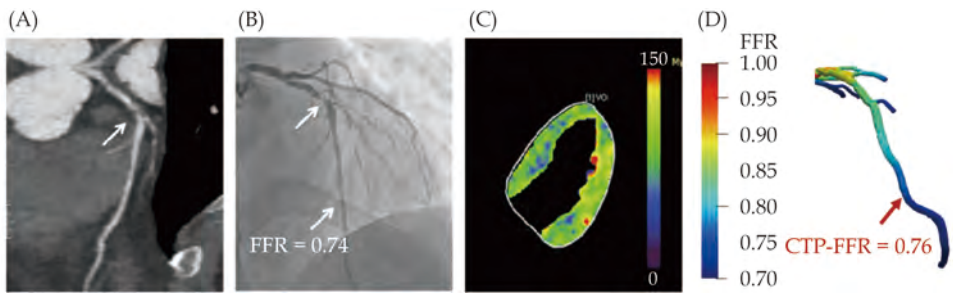

Figure 32 Example of a 47-year-old man who presented with atypical chest pain, hypertension and dyslipidemia. (A): CCTA shows stenosis (arrow) is caused by a mixed plaque of the proximal LAD; (B): invasive coronary angiography shows severe stenosis (arrow) with ischemia in LAD (FFR = 0.74); (C): stress-CTP shows myocardial blood flow; (D): CTP-FFR demonstrates value of 0.76 in the LAD. CCTA: coronary computed tomography angiography, CTP: CT perfusion, FFR: fractional flow reserve; LAD: left anterior descending. Reprinted with permission under open access from Go *et al*.[219]

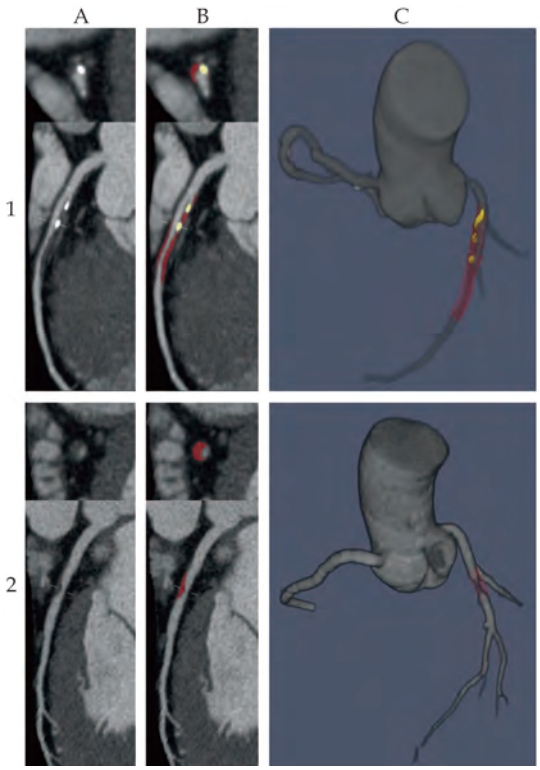

Figure 33 The use of deep learning for plaque segmentation. (A): Curved multiplanar reformation coronary CTA images showing lesions in the proximal-to-mid LAD (1) and the mid LAD (2); (B): deep learning segmentation of calcified plaque (yellow) and non-calcified plaque (red); (C): three-dimensionally rendered view of the coronary tree showing deep learning plaque segmentation in the individual analyzed segments. All lesions in each vessel were analyzed by deep learning and measurements summed on a per-patient level. CTA: computed tomography angiography; LAD: left anterior descending artery. Reprinted with permission under open access from Lin, *et al*.[231]

ent approaches have been explored to suppress the blooming artifacts with improved specificity and PPV to some extent, use of DL models has been shown to further enhance coronary CTA performance in calcified plaques. Figure 34 is an example of our recent work by applying advanced DL models to reduce the effect of blooming artifacts caused by calcified plaques with more accurate assessment of coronary stenosis. We are currently collecting more data to further validate the advanced DL models in the quantitative assessment of calcified plaques. [230]

AI Assisting Diagnosis of Pulmonary Hypertension

Another research work from our group and others is the development of a fully automated framework with use of AI to assist the diagnosis of pulmonary hypertension based on CT pulmonary angiography (CTPA) images.[229,237-239] There was good correlation between AI-based automatic extraction of anatomical features from CTPA and manual measurements (Figure 35). The accuracy of the regression model is comparable to the gold standard to predict pulmonary artery pressure.

SUMMARY AND FUTURE PERSPECTIVES

Cardiovascular CT has played a pivotal role in the routine clinical practice and already serves as the method of choice in the diagnosis of various cardiovascular diseases. The clinical value of cardiovascular CT has been significantly enhanced with use of CT-derived 3D visualisations as well as hemodynamic analysis of functional changes to the cardiovascular system. This leads to the paradigm shift in cardiovascular CT applications from diagnosis to prediction with eventual improvement in patient outcomes. In addition to the standard 2D or 3D CT image visualisations, 3D reconstructions such as generation of VIE views provide intraluminal changes associated with coronary plaques, aortic dissection, aortic stent wires and pulmonary embolism. Incorporation of coronary angle measurements into the standard measurement parameters further improves diagnostic accuracy of coronary CTA when compared to the standard lumen assessment in determining coronary artery disease, thus overcoming the limitations of coronary CTA in assessing calcified plaques. VR is also becoming a useful tool in many applications spanning across from medical education to surgical planning and clinical communication within health professionals. With more research to be conducted on the value of AR and MR, these 3D visualisation tools will continue to play an important role in complementing the traditional visualisations.

3D printed personalised models developed from CT images add incremental value of cardiovascular CT since the physical models provide users with more vivid visualisation of complex cardiovascular anatomy and pathology, in addition to the value of serving as a tool for both medical and clinical training of medical students/graduates, simulation of challenging cardiovascular procedures. The highly

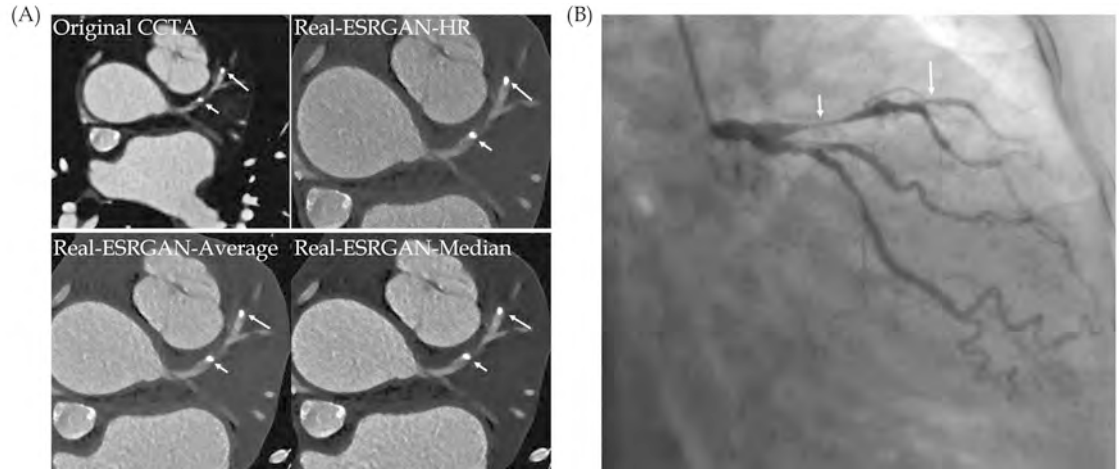

Figure 34 Multiple calcified plaques at the left anterior descending artery (LAD) in a 72-year-old female. (A): Coronary stenoses were measured at 80%, 78%, 72%, and 70% corresponding to the original CCTA, Real-ESRGAN-HR, Real-ESRGAN-Average and Real-ESRGAN-Median images (short arrows), respectively. (B): ICA (short arrow) confirms 75% stenosis. The distal stenoses at LAD due to calcified plaques were measured at 70%, 50%, and 51% stenosis on original CCTA, Real-ESRGAN-HR, and Real-ESRGAN-Average images but measured at 45% on Real-ESRGAN-Median images (long arrows in (A)). ICA confirmed the only 37% stenosis (long arrow in (B)). CCTA: coronary computed tomography angiography; ESRGAN: enhanced super-resolution generative adversarial network; HR: high resolution; ICA: invasive coronary angiography, Real-ESRGAN: real-enhanced super-resolution generative adversarial network. Reprinted with permission under open access from Sun and Ng.[230]

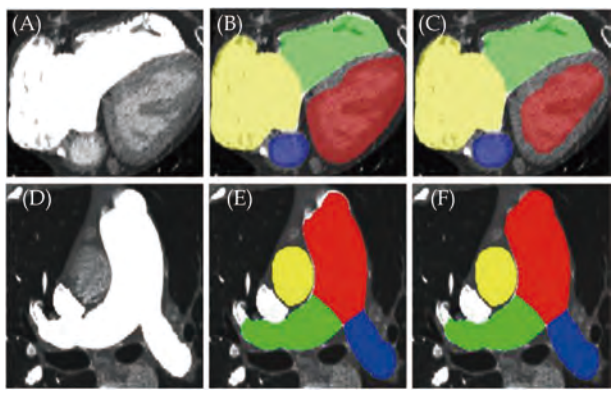

Figure 35 The performance of the proposed network framework. (A, D): The original images of the heart and pulmonary artery, respectively; (B, E): the segmentation outputs of nnU-Net; (C, F): the segmentation outputs of the proposed network framework. Segmented structures include right atrium (yellow), right ventricle (green), left atrium (blue), left ventricle (red), main pulmonary artery (red), right pulmonary artery (green) and left pulmonary artery (blue). Reprinted with permission under open access from Zhang, *et al.*[229]

accurate 3D printed models are advantageous to commercial phantoms to optimise CT scanning protocols because of low cost, representation of patient-specific anatomical structures. With further reduction of costs associated with 3D printers and printing materials, 3D printed cardiovascular models will be accessible to more clinical and research sites.

CT-derived flow dynamic analysis further advances the diagnostic value of cardiovascular CT by providing physiological changes associated with lesions which cannot be acquired from the standard lumen assessment. CFD analysis of coronary plaques or coronary angulation changes offers additional information about identification of vulnerable lesions such as high-risk coronary plaques, or prediction of disease outcomes as shown in type B aortic dissection through analysis of hemodynamic changes in the aortic lumen, in particular in the false lumen. FFRCT is another promising technique providing both anatomic and physiologic information of coronary plaques, further enhancing the diagnostic value of coronary CTA in coronary artery disease. FFRCT with aid of AI tools has become more efficient, and with refinement of AI algorithms it will be a routinely used onsite diagnostic tool to guide clinical management of patients with coronary artery disease.

Use of AI has been growing rapidly in the cardiovascular disease with evidence showing its capability to improve diagnostic accuracy and prediction of disease outcomes. In the field of cardiovascular disease, the role of AI is to support but not replace clinicians, assist clinical decision making but not make decisions. Therefore, it is important for clini-

Figure 36 The applications of artificial intelligence in clinical cardiology practice. CAC: coronary calcium score; CAD: coronary artery disease; EAT: epicardial adipose tissue; LV: left ventricle; PVAT: perivascular adipose tissue. Reprinted with permission under open access from Jiang *et al.* [240].

cians to be aware of it so that they know how to utilise AI judiciously and accurately to perform big data analysis, and maximize AI applications to deliver personalised medicine in cardiovascular disease. Figure 36 summarises the AI applications in cardiovascular medicine.[240]

REFERENCES

[1] Halliburton S, Arbab-Zadeh A, Dey D, *et al*. State-of-the-art in CT hardware and scan modes for cardiovascular CT. *J Cardiovasc Comput Tomogr* 2012; 6: 154–163.

[2] Gulsin GS, McVeigh N, Leipsic JA, Dodd JD. Cardiovascular CT and MRI in 2020: review of key articles. *Radiology* 2021; 301: 263–277.

[3] Schuleri KH, George RT, Lardo AC. Applications of cardiac multidetector CT beyond coronary angiography. *Nat Rev Cardiol* 2009; 6: 699–710.

[4] Sun Z. Helical CT angiography of abdominal aortic aneurysms treated with suprarenal stent grafting: a pictorial essay. *Cardiovasc Intervent Radiol* 2003; 26: 290–295.

[5] Sun Z, Lin CH, Davidson R, *et al*. Diagnostic value of 64-slice CT angiography in coronary artery disease: A systematic review. *Eur J Radiol* 2008; 67: 78–84.

[6] Sun Z, Ng KH, Vijayananthan A. Is use of computed tomography justified in clinical practice? Part I: Application in the emergency department. *Singapore Med J* 2010; 51: 200–206.

[7] Sun Z, Ng KH. Multislice CT angiography in the cardiac imaging: Part II: Diagnostic applications in coronary artery disease. *Singapore Med J* 2010; 51: 282–289.

[8] Sun Z, Ng KH. Multislice CT angiography in cardiac imaging: Part III: Radiation risk and dose reduction. *Singapore Med J* 2010; 51: 374–380.

[9] Sun Z, Ng KH, Sarji SA. Is use of computed tomography justified in clinical practice? Part IV: Application in paediatric imaging. *Singapore Med J* 2010; 51:

457–463.
[10] Sabarudin A, Sun Z, Ng KH. A systematic review of radiation dose associated with different generations of multislice CT coronary angiography. *J Med Imag Radiat Oncol* 2012; 56: 5–17.
[11] Sun Z. Computed tomography angiography in the diagnosis of cardiovascular disease: 3D visualisations. *Front Med* 2011; 5: 254–270.
[12] Sun Z, Cao Y, Li H. Multislice CT angiography in the diagnosis of coronary artery disease. *J Geriatr Cardiol* 2011; 8: 104–113.
[13] Sun Z. Abdominal aortic aneurysm: Treatment options, image visualizations and follow-up procedures. *J Geriatr Cardiol* 2012; 9: 49–60.
[14] Sun Z, Ng KH. Diagnostic value of coronary CT angiography with prospective ECG- gating in the diagnosis of coronary artery disease: A systematic review and meta-analysis. *Int J Cardiovasc Imaging* 2012; 28: 2109–2119.
[15] Sun Z, Choo GH, Ng KH. Coronary CT angiography: current status and continuing challenges. *Br J Radiol* 2012; 85: 495–510.
[16] Sun Z, Ng KH. Prospective versus retrospective ECG-gated multislice CT coronary angiography: A systematic review of radiation dose and image quality. *Eur J Radiol* 2012; 81: e94–e100.
[17] Sun Z, Faridah Y, Ng KH. Coronary CT angiography: How should physicians use it widely and when do physicians request it appropriately?. *Eur J Radiol* 2012; 81: e684–e687.
[18] Sun Z. Cardiac CT imaging: current status and future directions. *Quant Imaging Med Surg* 2012; 2: 98–105.
[19] Sabarudin A, Khairuddin Md Yusof A, *et al*. Dual-source CT coronary angiography: effectiveness of radiation dose reduction with lower tube voltage. *Radiat Prot Dosim* 2013; 153: 441–447.
[20] Sabarudin A, Sun Z, Ng KH. Coronary CT angiography with prospective ECG- triggering: A systematic review of image quality and radiation dose. *Singapore Med J* 2013; 54: 15–23.
[21] Sabarudin A, Sun Z, Khairuddin Md Yusof A. Coronary CT angiography with single- source and dual-source CT: Comparison of image quality and radiation dose between prospective ECG-triggered and retrospective ECG-gated protocols. *Int J Cardiol* 2013; 168: 746–753.
[22] Sun Z. Cardiac imaging in the diagnosis of coronary artery disease: a comprehensive review of various imaging modalities. *Curr Med Imaging Rev* 2013; 9: 167–169.
[23] Sun Z. Quantitative cardiovascular imaging. *Quant Imaging Med Surg* 2014; 4: 297–299.
[24] Sun Z, Lin C. Diagnostic value of 320-slice coronary CT angiography in coronary artery disease: A systematic review and meta-analysis. *Curr Med Imaging Rev* 2014; 10: 272–280.
[25] Sun Z, Almoudi M, Cao Y. CT angiography in the diagnosis of cardiovascular disease: A transformation in cardiovascular CT practice. *Quant Imaging Med Surg* 2014; 4: 376–396.
[26] Shen Y, Sun Z, Xu L, *et al*. High- pitch, low-voltage and low-iodine concentration CT angiography of aorta: assessment of image quality and radiation dose with iterative reconstruction. *Plos One* 2015; 10: 0117469.
[27] Almutairi A, Sun Z, Poovathumkadavi A, Assar T. Correction: Dual-energy CT angiography of peripheral arterial disease: feasibility of using lower contrast medium volume. *Plos One* 2015; 10: e0145976.
[28] Tan SK, Yeong CH, Ng KH, Abdul Aziz Y, Sun Z. Recent update on radiation dose assessment for the state-of-art coronary computed tomography angiography (CCTA) protocols. *Plos One* 2016; 11: e0161543.
[29] Liang J, Wang H, Xu L, *et al*. Diagnostic performance of a 256-row detector computed tomography in patients with high heart rates within a single cardiac cycle: A preliminary study. *Clin Radiol* 2017; 72: 694e7–694e14.
[30] Wang H, Xu L, Fan Z, Liang J, Yan Z, Sun Z. Clinical evaluation of new automatic coronary-specific best cardiac phase selection algorithm for single-beat coronary CT angiography. *Plos One* 2017; 12: e0172686.
[31] Wang R, Liu X, Schoepf UJ, *et al*. Extracellular volume quantification using dual-energy CT in patients with heart failure: comparison with 3T cardiac MR. *In J Cardiol* 2018; 268: 236–240.
[32] Tan S, Yeong CH, Aman R, *et al*. Low tube voltage prospectively ECG-triggered coronary CT angiography: A systematic review of image quality and radiation dose. *Br J Radiol* 2018; 91(1088): 20170874.
[33] Liang J, Sun Y, Ye Z, *et al*. Second generation motion correction algorithm improved diagnostic accuracy of single-beat coronary CT angiography in patients with increased heart rate. *Eur Radiol* 2019; 29: 4215–4227.
[34] Zhou Z, Xu L, Wang R, *et al*. Quantification of doxorubicin-induced interstitial myocardial fibrosis in a beagle model using equilibrium contrast-enhanced computed tomography: A comparative study with cardiac magnetic resonance T1-mapping. *Int J Cardiol* 2019; 281: 150–155.
[35] Tan SW, NG KH, Yeong CH, *et al*. Personalized administration of contrast medium with high delivery rate in low tube voltage coronary computed tomography angiography. *Quant Imaging Med Surg* 2019; 9: 552–564.
[36] Flohr T, Schmidt B, Ulzheimer S, Alkadhi H. Cardiac imaging with photon counting CT. *Br J Radiol* 2023; 96: 20230407.
[37] Cademartiri F, Meloni A, Pistoia L, *et al*. Dual-Source Photon-Counting Computed Tomography & mdash; Part I: Clinical Overview of Cardiac CT and Coronary CT Angiography Applications. *J Clin Med* 2023; 12: 3627.
[38] Si-Mohamed SA, Boccalini S, Lacombe H, *et al*. Coronary CT angiography with photon-counting CT: first-in-human results. *Radiology* 2022; 303: 303–313.
[39] Sun Z, Silberstein J, Vaccarezza M. Cardiovascular computed tomography in the diagnosis of cardiovascular disease: Beyond lumen assessment. *J Cardiovasc Dev Dis* 2024; 11: 22.
[40] Tonet E, Boccadoro A, Micillo M, *et al*. Coronary computed tomography angiography: beyond obstructive coronary artery disease. *Life (Basel)* 2023; 13: 1086.

[41] Thomas AC, Santos AL, Fragata J. Virtual angioscopy and 3D navigation of the aorta. *J Card Surg* 2017; 32: 33–37.
[42] Goo HW, Park SJ, Yoo SH. Advanced medical use of three-dimensional imaging in congenital heart disease: Augmented reality, mixed reality, virtual reality, and three-dimensional printing. *Korean J Radiol* 2020; 21: 133–145.
[43] Barteit S, Lanfermann L, Barnighausen T, *et al*. Augmented, mixed, and virtual reality-based hear-mounted devices for medical education: Systematic review. *JMRS Serious Games* 2021; 9: e29080.
[44] Sun Z, Xu L. Computational fluid dynamics in coronary artery disease. *Comput Med Imaging Graph* 2014; 38: 651–663.
[45] Raja J, Seitz MP, Yedlapati N, Khouzam RN. Can computed fractional flow reserve coronary angiography (FFRCT) offer an accurate noninvasive comparison to invasive coronary angiography (ICA)? "The noninvasive CATH". *A comprehensive review. Curr Probl Cardiol* 2021; 46: 100642.
[46] Chen J, Wetzel L, Pope KL, *et al*. FFRCT: current status. *AJR Am J Roentgenol* 2021; 216: 640–648.
[47] Morris PD, Narracott A, von Tengg-Kobligk H, *et al*. Computational fluid dynamics modelling in cardiovascular medicine. *Heart* 2016; 102: 18–28.
[48] Sandeep B, Liu X, Huang X, *et al*. Feasibility of artificial intelligence its current status, clinical applications and future direction in cardiovascular disease. *Curr Probl Cardiol* 2024; 49: 102349.
[49] Haq IU, Haq I, Xu B. Artificial intelligence in personalized cardiovascular medicine and cardiovascular imaging. *Cardiovasc Diagn Ther* 2021; 11: 911–923.
[50] Rajpurkar P, Chen E, Banerjee O, Topol EJ. AI in health and medicine. *Nat Med* 2022; 28: 31–38.
[51] Allmendinger T, Nowak T, Flohr T, *et al*. Photon-counting detector CT-based vascular calcium removal algorithm: Assessment using a cardiac motion phantom. *Invest Radiol* 2022; 57: 399–405.
[52] Meloni A, Frijia F, Panetta D, *et al*. Photon-counting computed tomography (PCCT): technical background and cardio-vascular applications. *Diagnostics* 2023; 13: 645.
[53] Hapsonik EF, Aquino SL, Vining DJ. Virtual bronchoscopy. *Clin Chest Med* 1999; 20: 201–217.
[54] Oto A. Virtual endoscopy. *Eur J Radiol* 2002; 42: 231–239.
[55] Ahmad I, Millhoff B, John M, Andi K, Oakley R. Virtual endoscopy-a new assessment tool in difficult airway management. *J Clin Anesth* 2015; 27: 508–513.
[56] Lefere P, Gryspeerdt S, Schotte K. Virtual colonoscopy-an overview. *Onkologie* 2006; 29: 281–286.
[57] Mirhosseini S, Gutenko I, Ojal S, *et al*. Immersive virtual colonoscopy. *IEEE Trans Vis Comput Graph* 2019; 25: 2011–2021.
[58] Chervenkov L, Sirakov N, Georgiev A, *et al*. High concordance of CT colonography and colonoscopy allows for the distinguishing and diagnosing of intestinal diseases. *Life (Basel)* 2023; 13: 1906.
[59] Neri E, Caramella D, Falaschi F, *et al*. Virtual CT intravascular endoscopy of the aorta: pierced surface and floating shape thresholding artifacts. *Radiology* 1999; 212: 276–279.
[60] Sun Z, Dimpudus F, Adipranoto JD, Nugroho J. CT virtual intravascular endoscopy assessment of coronary artery plaques: A preliminary study. *Eur J Radiol* 2010; 75: e112–e119.
[61] Sun Z, Xu L. CT virtual intravascular endoscopy in the visualization of coronary plaques: A pictorial essay. *Curr Med Imaging Rev* 2017; 13: 154–161.
[62] Xu L, Sun Z. Virtual intravascular endoscopy visualization of calcified coronary plaques: A novel approach of identifying plaque features for more accurate assessment of coronary lumen stenosis. *Medicine* 2015; 94: e805.
[63] Huseinagic H, Efendic A, Rusidovic I. 3D computed tomography intravascular endoscopy. *Pol J Radiol* 2023; 88: e435–e444.
[64] Wu PW, Tsay PK, Sun Z, *et al*. Added value of computed tomography virtual intravascular endoscopy in the evaluation of coronary arteries with stents or plaques. *Diagnostics* 2022; 12(2): 390.
[65] Sun Z, Winder J, Kelly B, *et al*. Assessment of VIE image quality using helical CT angiography: in vitro phantom study. *Comput Med Imaging Graph* 2004; 28: 3–12.
[66] Sun Z, Gallagher E. Multislice CT virtual intravascular endoscopy for abdominal aortic aneurysm stent grafts. *J Vasc Intervent Radiol* 2004; 15: 961–970.
[67] Sun Z, Ferris C. Optimal Scanning protocol of multislice CT virtual intravascular endoscopy in pre-aortic stent grafting: in vitro phantom study. *Eur J Radiol* 2006; 58: 310–316.
[68] Sun Z, Al Dosari S, Ng C, Al-Mumntshari A, Almaliky S. Multislice CT virtual intravascular endoscopy of pulmonary embolism: A pictorial review. *Korean J Radiol* 2010; 11: 222–230.
[69] Sun Z, Cao Y. Multislice CT virtual intravascular endoscopy of aortic dissection: a pictorial essay. *World J Radiol* 2010; 2: 440–448.
[70] Qi Y, Ma X, Li G, *et al*. Three-dimensional visualization and imaging of the entry tear and intimal flap of aortic dissection using CT virtual intravascular endoscopy. *PLoS One* 2016; 11: e0164750.
[71] Sun Z. Three-Dimensional visualization of suprarenal aortic tent-grafts: Evaluation of migration in midterm follow-up. *J Endovasc Ther* 2006; 1: 85–93.
[72] Sun Z. 3D multislice CT angiography in post-aortic stent grafting: A pictorial essay. *Korean J Radiol* 2006; 7: 205–211.
[73] Sun Z, Winder J, Kelly B, *et al*. Diagnostic value of CT virtual intravascular endoscopy in aortic stent grafting. *J Endovasc Ther* 2004; 11: 13–25.
[74] Sun Z, Zheng H. Cross-sectional area reduction of the renal ostium by suprarenal stent wires: in vitro phantom study by CT virtual angioscopy. *Comput Med Imaging Graph* 2004; 28: 345–351.
[75] Sun Z, Zheng H. Effect of suprarenal stent struts on the renal ostia with ostial calcification observed in CT virtual intravascular endoscopy. *Eur J Vasc Endovasc Surg* 2004; 28: 534–542.
[76] Sun Z. Transrenal fixation of aortic stent grafts: cur-

rent status and future directions. *J Endovasc Ther* 2004; 11: 539–549.
[77] Sun Z, Winder J, Kelly B, Ellis P, Hirst D. CT virtual intravascular endoscopy of abdominal aortic aneurysms treated with suprarenal endovascular stent grafting. *Abdom Imaging* 2003; 28: 580–587.
[78] Sun Z, O'Donnell M, Winder R, Ellis P, Blair P. Effect of suprarenal fixation of aortic stent grafts on renal ostium: Assessment of morphological changes by virtual intravascular endoscopy. *J Endovasc Ther* 2007; 14: 650–660.
[79] Sun Z, Allen Y, Nadkarni S, *et al*. CT virtual intravascular endoscopy in the visualization of fenestrated endovascular grafts. *J Endovasc Ther* 2008; 15: 42–51.
[80] Sun Z, Allen Y, Mwipatayi B, Hartley D, Lawrence-Brown M. Multislice CT angiography in the follow-up of fenestrated endovascular grafts: Effect of slice thickness on 2D and 3D visualization of the fenestrated stents. *J Endovasc Ther* 2008; 15: 417–426.
[81] Sun Z. Multislice CT angiography in post-aortic stent grafting: optimization of scanning protocols for virtual intravascular endoscopy. *Int J Comput Assist Radiol Surg* 2008; 3: 19–26.
[82] Sun Z, Allen Y, Mwipatayi B, Hartley D, Lawrence-Brown M. Multislice CT angiography of fenestrated endovascular stent grafting of abdominal aortic aneurysms: A pictorial review of 2D/3D visualizations. *Korean J Radiol* 2009; 10: 285–293.
[83] Sun Z, Mwipatayi B, Allen Y, Hartley D, Lawrence-Brown M. Multislice CT virtual intravascular endoscopy in the evaluation of fenestrated stent graft repair of abdominal aortic aneurysms: A short-term follow-up. *ANZ J Surg* 2009; 79: 836–840.
[84] Sun Z, Ng C. Dual source CT angiography in aortic stent grafting: An in vitro aorta phantom study of image noise and radiation dose. *Acad Radiol* 2010; 17: 884–893.
[85] Sun Z, Ng CK, Sa dos Reis C. Synchrotron radiation computed tomography versus conventional computed tomography for assessment of four types of stent grafts used for endovascular treatment of thoracic and abdominal aortic aneurysms. *Quant Imaging Med Surg* 2018; 8: 609–620.
[86] England A, Butterfield JS, Ashleigh RJ. Incidence and effect of bare suprarenal stent struts crossing renal ostia following EVAR. *Eur J Vasc Endovasc Surg* 2006; 32: 523–528.
[87] Sun Z, Ng CKC. High calcium scores in coronary CT angiography: effects of image post-processing on visualization and measurement of coronary lumen diameter. *J. Med Imaging Health Inform* 2015; 5: 110–6.
[88] Li P, Xu L, Yang L, *et al*. Blooming artifact reduction in coronary artery calcification by a new de-blooming algorithm: initial study. *Sci Rep* 2018; 8: 6945.
[89] Weir-McCall JR, Wang R, Halankar J, *et al*. Effect of a calcium deblooming algorithm on accuracy of coronary computed tomography angiography. *J Cardiovasc Comput Tomogr* 2020; 14: 131–6.
[90] Yunaga H, Ohta Y, Kaetsu Y, *et al*. Diagnostic performance of calcification-suppressed coronary CT angiography using rapid kilovolt-switching dual-energy CT. *Eur Radiol* 2017; 27: 2794–2801.
[91] Sun Z, Cao Y. Multislice CT angiography assessment of left coronary artery: correlation between bifurcation angle and dimensions and development of coronary artery disease. *Eur J Radiol* 2011; 79: e90–95.
[92] Sun Z. Coronary CT angiography in coronary artery disease: correlation between virtual intravascular endoscopic appearances and left bifurcation angulation and coronary plaques. *Biomed Res Int* 2013; 2013: 732059.
[93] Xu L, Sun Z. Coronary CT angiography evaluation of calcified coronary plaques by measurement of left coronary bifurcation angle. *Int J Cardiol* 2015; 18: 229–231.
[94] Temov K, Sun Z. Coronary computed tomography angiography investigation of the association between left main coronary artery bifurcation angle and risk factors with regard to the development of coronary artery disease. *Int J Cardiovasc Imaging* 2016; 32(Suppl 1): S129–S137.
[95] Juan Y, Tsay P, Shen W, *et al*. Comparison of the left main coronary bifurcating angle among patients with normal, non-significantly and significantly stenosed left coronary arteries. *Sci Rep* 2017; 7: 1515–1518.
[96] Cui Y, Zeng W, Yu J, *et al*. Quantification of left coronary bifurcation angles and plaques by coronary computed tomography angiography for prediction of significant coronary stenosis: A preliminary study with dual-source CT. *PLoS ONE* 2017; 12: e0174352.
[97] Liu Z, Zhao S, Li Y, *et al*. Influence of coronary bifurcation angle on atherosclerosis. *Acta Mech Sin* 2019; 35: 1269–1278.
[98] Moon S, Byun J, Kim J, *et al*. Clinical usefulness of the angle between left main coronary artery and left anterior descending coronary artery for the evaluation of obstructive coronary artery disease. *PLoS ONE* 2018; 13: e0202249.
[99] Sun Z, Xu L, Fan Z. Coronary CT angiography in calcified coronary plaques: Comparison of diagnostic accuracy between bifurcation angle measurement and coronary lumen assessment for diagnosing significant coronary stenosis. *Int J Cardiol* 2016; 203: 78–86.
[100] Givehchi S, Safari MJ, Tan S, *et al*. Measurement of coronary bifurcation angle with coronary CT angiography: A phantom study. *Phys Med* 2018; 45: 198–204.
[101] Geerlings-Batt J, Sun Z. Evaluation of the relationship between left coronary artery bifurcation angle and coronary artery disease: A systematic review. *J Clin Med* 2022; 11: 5143.
[102] Geerlings-Batt J, Sun Z. Coronary computed tomography angiography assessment of relationship between right coronary artery-aorta angle and the development of coronary artery disease. *Quant Imaging Med Surg* 2023; 13: 1948–1956.
[103] Geerlings-Batt J, Gupta A, Sun Z. Investigation of the relationship between right coronary artery-aorta angle and coronary artery disease and associated risk factors. *J Clin Med* 2023; 12(3): 1051.
[104] Sun Z, Squelch A, Bartlett A, Cunningham K, Lawrence-Brown M. 3D stereoscopic visualization in fenestrated stent grafts. *Cardiovasc Intervent Radiol*

2009; 32: 1053−1058.
[105] Javvaji CK, Reddy H, Vagha JD, *et al*. Immersive innovations: exploring the diverse applications of virtual reality (VR) in healthcare. *Cureus* 2024; 16: e56137.
[106] Geerlings-Batt, Tillett C, Gupta A, Sun Z. Enhanced visualisation of normal anatomy with augmented reality superimposed on three-dimensional printed models. *Micromachines* 2022; 13(10): 1701.
[107] Gehrsitz P, Rompel O, Schöber M, *et al*. Cinematic rendering in mixed-reality holograms: A new 3D preoperative planning tool in pediatric heart surgery. *Front Cardiovasc Med* 2021; 8: 633611.
[108] Ye W, Zhang X, Li T, Luo C, Yang L. Mixed-reality hologram for diagnosis and surgical planning of double outlet of the right ventricle: A pilot study. *Clin Radiol* 2021; 76: 237. e.
[109] Kumar RP, Pelanis E, Bugge R, *et al*. Use of mixed reality for surgery planning: Assessment and development workflow. *J Biomed Inform* 2020; 112: 100077.
[110] Jung C, Wolff G, Wernly B, *et al*. Virtual and augmented reality in cardiovascular care: State-of-the-art and future perspectives. *JACC Cardiovasc. Imaging* 2022; 15: 519−532.
[111] Banerjee S, Pham T, Eastaway A, Auffermann WF, Quigley III EP. The use of virtual reality in teaching three-dimensional anatomy and pathology on CT. *J Digit Imaging* 2023; 36: 1279−1284.
[112] Zhao J, Xu X, Jiang H, Ding Y. The effectiveness of virtual reality-based technology on anatomy teaching: a meta-analysis of randomized controlled studies. *BMC Med Educ* 2020; 20: 17.
[113] Uruthiralingham U, Rea PM. Augmented and virtual reality in anatomical education- A systematic review. *Adv Exp Med Biol* 2020; 1235: 89−101.
[114] Moro C, Birt J, Stromberga Z, *et al*. Virtual and augmented reality enhancements to medical and science student physiology and anatomy test performance: A systematic review and meta-analysis. *Anat Sci Educ* 2021; 14: 368−376.
[115] Lau I, Gupta A, Sun Z. Clinical value of virtual reality versus 3D printing in congenital heart disease. *Biomolecules* 2021; 11: 884.
[116] Lau I. Gupta A, Ihdayhid A, Sun Z. *Clinical applications of mixed reality and 3D printing in congenital heart disease. Biomolecules* 2022; 12: 1548.
[117] Lau I, Wong YH, Yeong CH, *et al*. Quantitative and qualitative comparison of low- and high-cost 3D-printed heart models. *Quant Imaging Med Surg* 2019; 9: 107−114.
[118] Lau I, Sun Z. Dimensional accuracy and clinical value of 3D printed models in congenital heart disease: A systematic review and meta-analysis. *J Clin Med* 2019; 8: 1483.
[119] Lee S, Squelch A, Sun Z. Quantitative assessment of 3D printed model accuracy in delineating congenital heart disease. *Biomolecules* 2021; 11: 270.
[120] Gharleghi R, Dessalles CA, Lal R, *et al*. 3D printing for cardiovascular applications: from end-to-end processes to emerging developments. *Ann Biomed Eng* 2021; 49: 1598−1618.
[121] Gardin C, Ferroni L, Latremouille C, *et al*. Recent applications of three dimensional printing in cardiovascular medicine. *Cells* 2020; 9: 742.
[122] Sun Z. 3D printing in medicine: current applications and future directions. Quant Imaging Med Surg 2018: 8: 1069-1077.
[123] Sun Z. Insights into 3D printing in medical applications. *Quant Imaging Med Surg* 2019; 9: 1−5.
[124] Sun Z. Clinical applications of patient-specific 3D printed models in cardiovascular disease: current status and future directions. *Biomolecules* 2020; 10: 1577.
[125] Sun Z, Wee C. 3D printed models in cardiovascular disease: An exciting future to deliver personalized medicine. *Micromachines* 2022; 13(10): 1575.
[126] Vukicevic M, Mosadegh B, Min JK, Little SH. 3D printing and its future directions. *JACC Cardiovasc Imaging* 2017; 10: 171−134.
[127] Sun Z, Zhao J, Leung E, *et al*. 3D bioprinting in cardiovascular disease: current status and future directions. *Biomolecules* 2023; 13: 1180.
[128] Zhang Y, Kumarwew P, Lv S, *et al*. Recent advances in 3D bioprinting of vascularized tissues. *Mater Des* 2021; 199: 109398.
[129] Alonzo M, Anilkumar S, Roman B, Tasnim N, Joddar B. 3D bioprinting of cardiac tissue and cardiac stem cell therapy. *Transl Res* 2019; 211: 64−83.
[130] Gomez-Ciriza G, Gomex-Cia T, Rivas-Gonzalez JA, *et al*. Affordable three-dimensional printed heart models. *Front Cardiovasc Med* 2021; 8: 642011.
[131] Ho D, Squelch A, Sun Z. Modelling of aortic aneurysm and aortic dissection through 3D printing. *J Med Radiat Sc* 2017; 64: 10−17.
[132] Sun Z, Squelch A. Patient-specific 3D printed models of aortic aneurysm and aortic dissection. *J Med Imaging Health Inf* 2017; 7: 886−889.
[133] Lau I, Sun Z. Three-dimensional printing in congenital heart disease: A systematic review. *J Med Radiat Sc* 2018; 65: 226−236.
[134] Perica E, Sun Z. Patient- specific three-dimensional printing for pre-surgical planning in hepatocellular carcinoma treatment. *Quant Imaging Med Surg* 2017; 7: 668−677.
[135] Sun Z, Liu D. A systematic review of three-dimensional printing in renal disease. *Quant Imaging Med Surg* 2018; 8: 311−325.
[136] Perica E, Sun Z. A systematic review of three-dimensional printing in liver disease. *J Digit Imaging* 2018; 31: 692−701.
[137] Sun Z, Ng CK, Squelch A. Synchrotron radiation computed tomography assessment of calcified plaques and coronary stenosis with different slice thicknesses and beam energies on 3D printed coronary models. *Quant Imaging Med Surg* 2019; 9: 6−22.
[138] Witowski J, Wake N, Grochowska A, *et al*. Investigating accuracy of 3d printed liver models with computed tomography. *Quant Imaging Med Surg* 2019; 9: 43−52.
[139] Allan A, Kealley K, Squelch A, *et al*. Patient-specific 3D printed model of biliary ducts with congenital cyst. *Quant Imaging Med Surg* 2019; 9: 86−93.
[140] Lupulescu C, Sun Z. A systematic review of the clinical value and application of three-dimensional print-

ing in renal disease. *J Clin Med* 2019; 8: 990.
[141] Sindi R, Sa Dos Reis C, Bennett C, Stevenson G, Sun Z. Quantitative measurements of breast density using magnetic resonance imaging: A systematic review and meta-analysis. *J Clin Med* 2019; 8: 745.
[142] Sun Z, Lau I, Wong YH, Yeong CH. Personalised three-dimensional printed models in congenital heart disease. *J Clin Med* 2019; 8: 522.
[143] Sun Z. 3D printed coronary models offer new opportunities for developing optimal coronary CT angiography protocols in imaging coronary stents. *Quant Imaging Med Surg* 2019; 9: 1350–1355.
[144] Etherton D, Tee L, Tillett C, Wong YH, Yeong CH, Sun Z. 3D visualization and 3D printing in abnormal gastrointestinal system manifestations of situs ambiguous. *Quant Imaging Med Surg* 2020; 10: 1877–1983.
[145] Sindi R, Wong YH, Yeong CH, Sun Z. Quantitative measurement of breast density using personalized 3D-printed breast model for magnetic resonance imaging. *Diagnostics* 2020; 10: 793.
[146] Sindi R, Wong YH, Yeong CH, Sun Z. Development of patient-specific 3D-printed breast phantom using silicone and peanut oils for magnetic resonance imaging. *Quant Imaging Med Surg* 2020; 10: 1237–1248.
[147] Wu C, Squelch A, Sun Z. Optimal image segmentation protocol for three-dimensional printing of aortic dissection through open-source software. *3D Print Med* 2021; 5: 37–49.
[148] Chessa M, Van de Bruaene A, Farooqi K, *et al*. 3D printing, holograms, computational modeling and artificial intelligence for adult congenital heart disease care: an exciting future. *Eur Heart J* 2022; 43: 2672–2684.
[149] Sun Z. Patient-specific 3D printed models in pediatric congenital heart disease. *Children* 2023; 10(2): 319.
[150] Sun Z, Wong YH, Yeong CH. Patient-specific 3D printed low-cost models in medical applications. *Micromachines* 2023; 14(2): 464.
[151] Wu C, Squelch A, Sun Z. Investigation of three-dimensional printing materials for printing aorta model replicating type B aortic dissection. *Curr Med Imaging* 2021; 17: 843–849.
[152] Wu C, Squelch A, Jansen S, Sun Z. Optimization of computed tomography angiography protocols for follow-up Type B aortic dissection patients by using 3D printed model. *Appl Sci* 2021; 11(15): 6844.
[153] Sun Z, Ng CKC, Wong YH, Yeong CH. 3D-printerd coronary plaques to simulate high calcification in the coronary arteries for investigation of blooming artifacts. *Biomolecules* 2021; 11: 1307.
[154] Sun Z. 3D printed coronary models offer potential value in visualising coronary anatomy and coronary stents for investigation of coronary CT protocols. *Curr Med Imaging* 2020; 16: 625–628.
[155] Aldosari S, Jansen S, Sun Z. Patient-specific 3D printed pulmonary artery model with simulation of peripheral pulmonary embolism for developing optimal computed tomography pulmonary angiography protocols. *Quant Imaging Med Surg* 2019; 9: 75–85.
[156] Aldosari S, Jansen S, Sun Z. Optimization of computed tomography pulmonary angiography protocols using 3D printing model with simulation of pulmonary embolism. *Quant Imaging Med Surg* 2019; 9: 53–62.
[157] Sun Z, Jansen S. Personalized 3D printed coronary models for coronary stenting. *Quant Imaging Med Surg* 2019; 9: 1356–1367.
[158] Wu C, Squelch A, Sun Z. Assessment of optimization of CTA protocols for follow-up Type B aortic dissection patients by using 3D printed model. *J 3D Print Med* 2022; 6: 117–127.
[159] Abdullah KA, McEntee MF, Reed W, Kench PL. Development of an organ-specific insert phantom generated using a 3D printer for investigations of cardiac computed tomographic protocols. *J Med Radiat Sci* 2018; 65: 175–183.
[160] Morup SD, Stowe J, Precht H, Gervig MH, Foley S. Design of a 3D printed coronary artery model for CT optimization. *Radiography* 2022; 28: 426–432.
[161] Biglino G, Milano EG, Capelli C, *et al*. Three-dimensional printing in congenital heart disease: Considerations on training and clinical implementation from a teaching session. *Int JArtif Organs* 2019; 42: 595–599.
[162] Loke YH, Harahsheh AS, Krieger A, Olivieri LJ. Usage of 3D models of tetralogy of Fallot for medical education: Impact on learning congenital heart disease. *BMC Med Educ* 2017; 17: 54–61.
[163] Lim KHA, Loo ZY, Goldie SJ, Adams JW, McMenamin PG. Use of 3D printed models in medical education: A randomized control trial comparing 3D prints versus cadaveric materials for learning external cardiac anatomy. *Anat Sci Educ* 2015; 9: 213–221.
[164] Smerling J, Marboe CC, Lefkowitch JH, *et al*. Utility of 3D printed cardiac models for medical student education in congenital heart disease: Across a spectrum of disease severity. *Pediatr Cardiol* 2019; 40: 1258–1265.
[165] Su W, Xiao Y, He S, Huang P, Deng X. Three-dimensional printing models in congenital heart disease education for medical students: A controlled comparative study. *BMC Med Educ* 2018; 18: 178.
[166] Valverde I, Gomez G, Byrne N, *et al*. Criss-cross heart three-dimensional printed models in medical education: A multicentre study on their value as a supporting tool to conventional imaging. *Anat Sci Educ* 2022; 15: 719–730.
[167] Mogali SR, Chandrasekaran R, Radzi S, *et al*. Investigating the effectiveness of three-dimensionally printed anatomical models compared with plastinated human specimens in learning cardiac and neck anatomy: A randomized crossover study. *Anat Sci Educ* 2022; 15: 1007–1017.
[168] Arango S, Gorbaty B, Brigham J, Iaizzo PA, Perry TE. A role for ultra-high resolution three-dimensional printed human heart models. *Echocardiography* 2023; 40: 703–710.
[169] Illmann CF, Hosking M, Harris KC. Utility and Access to 3-Dimensional printing in the context of congenital heart disease: An international physician survey study. *CJC Open* 2020; 2: 207–213.
[170] Valverde I, Gomez-Ciriza G, Hussain T, *et al*. Three-dimensional printed models for surgical planning of

complex congenital heart defects: An international multicentre study. *Eur J Cardio-Thoracic Surg* 2017; 52: 1139–1148.
[171] Ryan J, Plasencia J, Richardson R, *et al*. 3D printing for congenital heart disease: A single site's initial three-year experience. *3D Print Med* 2018; 4: 10.
[172] Zhao L, Zhou S, Fan T, *et al*. Three-dimensional printing enhances preparation for repair of double outlet right ventricular surgery. *J Card Surg* 2018; 33: 24–27.
[173] DeCampos D, Teixeira R, Saleiro C, *et al*. 3D printing for left atrial appendage closure: A meta-analysis and systematic review. *Int J Cardiol* 2022; 356: 38–43.
[174] Xu JJ, Luo YJ, Wang JH, *et al*. Patient-specific three-dimensional printed heart models benefit preoperative planning for complex congenital heart disease. *World J Pediatr* 2019; 15: 246–254.
[175] Forte MNV, Hussain T, Roest A, *et al*. Living the heart in three dimensions: applications of 3D printing in CHD. *Cardiol Young* 2019; 29: 733–743.
[176] Biglino G, Koniordou D, Gasparini M, *et al*. Piloting the use of patient-specific cardiac models as a novel tool to facilitate communication during clinical consultations. *Pediatr Cardiol* 2017; 38: 813–818.
[177] Biglino G, Capelli C, Wray J, *et al*. 3D-manufactured patient-specific models of congenital heart defects for communication in clinical practice: feasibility and acceptability. *BMJ Open* 2015; 5: e007165.
[178] Biglino G, Moharem-Elgamal S, Lee M, Tulloh R, Caputo, M. The perception of a three-dimensional-printed heart model from the perspective of different stakeholders: A complex case of truncus arteriosus. *Front Pediatr* 2017; 5: 209.
[179] Sun Z, Chaichana T. Investigation of hemodynamic effect of stent wires on renal arteries in patients with abdominal aortic aneurysms treated with suprarenal stent grafts. *Cardiovasc Interv Radiol* 2009; 32: 647–657.
[180] Chaichana T, Sun Z, Jewkes J. Computation of haemodynamics in the left coronary artery with variable angulations. *J Biomech* 2011; 44: 1869–1878.
[181] Chaichana T, Sun Z, Jewkes J. Computational fluid dynamic analysis of the effect of plaques in the left coronary artery. *Comput Math Meth Med* 2012; 2012: 504367.
[182] Lawrence-Brown M, Stanley B, Sun Z, Semmens JB, Liffman K. Stress and strain behaviour modelling of the carotid bifurcation. *ANZ J Surg* 2011; 81: 810–816.
[183] Wong KL, Thavornpattanappong P, Cheng S, Sun Z, Tu J. Effect of calcification on the mechanical stability of plaque based on a three-dimensional carotid bifurcation model. *BMC Cardiovasc Disord* 2012; 12: 7.
[184] Wong KL, Sun Z, Worthley SG, Mazumdar J, Abbott D. Medical image diagnostics based on computer-aided flow analysis using magnetic resonance images. *Comput Med Imaging Graph* 2012; 36: 527–541.
[185] Wong KL, Sun Z, Tu J. Medical imaging and computer-aided flow analysis of a heart with an atrial septal defect. *J Mech Med Biol* 2012; 12: 5.
[186] Wan Ab Naim N, Ganesan PB, Sun Z, *et al*. Prediction of thrombus formation using vertical structures presentation in Stanford type B aortic dissection: A preliminary study using CFD approach. *Appl Math Model* 2016; 40: 3115–3127.
[187] Sun Z, Chaichana T. A systematic review computational fluid dynamics in type B aortic dissection. *Int J Cardiol* 2016; 210: 28–31.
[188] Sun Z, Chaichana T. Computational fluid dynamic analysis of calcified coronary plaques: correlation between hemodynamic changes and cardiac image analysis based on left coronary bifurcation angle and lumen assessments. *Interv Cardiol* 2016; 8: 713–719.
[189] Chong A, Doyle B, Jansen S, Ponosh S, Cissoni J, Sun Z. Blood flow velocity prediction in aortic stent grafts using computational fluid dynamics and Taguchi method. *Comput Biol Med* 2017; 84: 235–246.
[190] Sun Z, Chaichana T. An investigation of correlation between left coronary bifurcation angle and hemodynamic changes in coronary stenosis by coronary computed tomography-derived computational fluid dynamics. *Quant Imaging Med Surg* 2017; 7: 537–548.
[191] Wan Ab Naim WN, Ganesan PB, Sun Z, *et al*. Flow pattern analysis in type B aortic dissection patients after stent-grafting repair: comparison between complete and incomplete false lumen thrombosis. *Int J Numer Method Biomed Eng* 2018; 34: e2961.
[192] Wan Ab Naim WN, Sun Z, Liew YM, *et al*. Comparison of diametric and volumetric changes in Stanford Type B aortic dissection patients in assessing aortic remodeling post-stent treatment treat. *Quant Imaging Med Surg* 2021; 11: 1723–1736.
[193] Chong A, Sun Z, van de Velde L, *et al*. Hemodynamic comparison of AFX stent-graft and CERAB configuration for treatment of aortoiliac occlusive disease. *J Endovasc Ther* 2021; 28: 623–635.
[194] Armour CH, Guo B, Saitta S, *et al*. Evaluation and verification of patient-specific modelloig of type B aortic dissection. *Comput Biol Med* 2022; 140: 105033.
[195] Girardin L, Stokes C, Thet MS, *et al*. Patient-specific haemodynamic analysis of virtual grafting strategies in type B aortic dissection: impact of compliance mismatch. Cardiovasc Eng Technol 2024 Mar 4. doi: 10.1007/s13239-024-00713-6. Online ahead of print.
[196] Chong MY, Gu B, Armour CH, *et al*. An integrated fluid-structure interaction and thrombosis model for type B aortic dissection. *Biomech Model Mechanobiol* 2022; 21: 261–275.
[197] Stokes C, Ahmed D, Ling N, *et al*. Aneurysmal growth in type B aortic dissection: assessing the impact of patient-specific inlet conditions on key haemodynamic indices. *J Ro Soc Interface* 2023; 20: 20230281.
[198] Chaichana T, Sun Z, Jewkes J. Hemodynamic impacts of various types of stenosis in the left coronary artery bifurcations: A patient-specific analysis. *Phys Medica* 2013; 29: 447–452.
[199] Chaichana T, Sun Z, Jewkes. Haemodynamic analysis of the effect of different types of plaque at the left coronary artery. *Comput Med Imaging Graph* 2013; 37: 197–206.
[200] Chaichana T, Sun Z, Jewkes J. Hemodynamic impacts of left coronary stenosis: A patient-specific analysis. *Acta Bioeng Biomech* 2013; 15: 107–112.
[201] Wan Ab Naim N, Ganesan PB, Sun Z, Osman K, Lim

E. The impact of the number of tears in patient-specific Stanford type B aortic dissecting aneurysm: CFD simulation. *J Mech Med Biol* 2014; 14: 1450017.
[202] Chaichana T, Sun Z, Jewkes J. Impact of plaques in the left coronary artery on wall shear stress and pressure gradient in coronary side branches. *Comput Med Biomech Biomed Eng* 2014; 17: 108–118.
[203] Song Q, Chen M, Shang J, Hu Z, Cai H. Analysis of predictive model of coronary vulnerable plaque under hemodynamic numerical simulation. *J Healthc Eng* 2022; 2022: 3434910.
[204] Hakim, D, Coskun AU, Maynard C, *et al*. Endothelial shear stress computed from computed tomography angiography: A direct comparison to intravascular ultrasound. *J Cardiovasc Comput Tomogr* 2023; 17: 201–210.
[205] Tufaro V, Torii R, Erdogan E, *et al*. An automated software for real-time quantification of wall shear stress distribution in quantitative coronary angiography data. *Int J Cardiol* 2022; 357: 14–19.
[206] Pijls NHJ, Van Schaardenburgh P, De Bruyne B, *et al*. Percutaneous coronary intervention of functionally nonsignificant stenosis: 5-year follow-up of the DEFER Study. *J Am Coll Cardiol* 2007; 49: 2105–2111.
[207] Zimmermann FM, Ferrara A, Johnson NP, *et al*. Deferral vs. performance of percutaneous coronary intervention of functionally non-significant coronary stenosis: 15-year follow-up of the DEFER trial. *Eur Heart J* 2015; 36: 3182–3188.
[208] Tonino PAL, De Bruyne B, Pijls NHJ, *et al*. Fractional Flow Reserve versus Angiography for Guiding Percutaneous Coronary Intervention. *N Eng J Med* 2009; 360: 213–224.
[209] Nørgaard BL, Leipsic J, Gaur S, *et al*. Diagnostic Performance of Noninvasive Fractional Flow Reserve Derived from Coronary Computed Tomography Angiography in Suspected Coronary Artery Disease. *J Am Coll Cardiol* 2014; 63: 1145–1155.
[210] Colleran R, Douglas PS, Hadamitzky M, *et al*. An FFRCT diagnostic strategy versus usual care in patients with suspected coronary artery disease planned for invasive coronary angiography at German sites: One-year results of a subgroup analysis of the PLATFORM (Prospective Longitudinal Trial of FFRCT: Outcome and Resource Impacts) study. *Open Heart* 2017; 4: e000526.
[211] Douglas PS, Pontone G, Hlatky MA, *et al*. Clinical outcomes of fractional flow reserve by computed tomographic angiography-guided diagnostic strategies vs. usual care in patients with suspected coronary artery disease: The prospective longitudinal trial of FFRCT: Outcome and resource impacts study. *Eur Heart J* 2015; 36: 3359–3367.
[212] Patel MR, Nørgaard BL, Fairbairn TA, *et al*. 1-Year Impact on Medical Practice and Clinical Outcomes of FFRCT. *JACC Cardiovasc Imaging* 2020; 13: 97–105.
[213] Curzen NP, Nolan J, Zaman AG, Nørgaard BL, Rajani R. Does the routine availability of CT–derived FFR influence management of patients with stable chest pain compared to CT angiography alone? The FFRCT RIPCORD Study. *JACC Cardiovasc Imaging* 2016; 9: 1188–1194.
[214] Curzen N, Nicholas Z, Stuart B, *et al*. Fractional flow reserve derived from computed tomography coronary angiography in the assessment and management of stable chest pain: The FORECAST randomized trial. *Eur Heart J* 2021; 42: 3844–3852.
[215] Yang J, Shan D, Wang X, *et al*. On- Site Computed tomography-derived fractional flow reserve to guide management of patients with stable coronary artery disease: The TARGET Randomized Trial. *Circulation* 2023; 147: 1369–1381.
[216] Yang L, Xu L, He J, *et al*. Diagnostic performance of a fast non-invasive fractional flow reserve derived from coronary CT angiography: an initial validation study. *Clin Radiol* 2019; 74: 973. e1–973. e6.
[217] Gao Y, Wang W, Wang H, *et al*. Impact of sublingual nitroglycerin on the assessment of computed tomography-derived fractional flow reserve: An intraindividual comparison study. *J Comput Assist Tomogr* 2022; 6: 23–28.
[218] Gao X, Zhou Z, Gao Y, Sun Z, Xu L. Noninvasive fractional flow reserve derived from computed tomography angiography in a patient with abnormal origin of the left main artery and cardiac death. *Quant Imaging Med Surg* 2023; 13: 5374–5378.
[219] Gao X, Wang R, Sun Z, *et al*. A novel CT perfusion-based fractional flow reserve algorithm for detecting coronary artery disease. *J Clin Med* 2023; 12(6): 2154.
[220] Qiao HY, Tang CX, Schoepf UJ, *et al*. Impact of machine learning-based coronary computed tomography angiography fractional flow reserve on treatment decisions and clinical outcomes in patients with suspected coronary artery disease. *Eur Radiol* 2020; 30: 5841–5851.
[221] Liu X, Mo X, Zhang H, *et al*. A 2-year investigation of the impact of the computed tomography-derived fractional flow reserve calculated using a deep learning algorithm on routine decision-making for coronary artery disease management. *Eur Radiol* 2021; 31: 7039–7046.
[222] Lin A, Kolossvary M, Motwani M, *et al*. Artificial intelligence in cardiovascular CT: current status and future implications. *J Cardiovasc Comput Tomogr* 2021; 15: 462–469.
[223] Han D, Liu J, Sun Z, Cui Y, He Y, Yang Z. Deep learning analysis in coronary computed tomographic angiography imaging for the assessment of patients with coronary artery stenosis. *Comput Methods Programs Biomed* 2020; 196: 105651.
[224] Wang W, Wang H, Chen Q, *et al*. Coronary artery calcium score quantification using a deep learning algorithm. *Clin Radiol* 2020; 75: 237e11–237e16.
[225] Sun Z, Ng CKC. Artificial intelligence (Enhanced Super-Resolution Generative Adversarial Network) for calcium deblooming in coronary computed tomography. *Diagnostics* 2022; 12: 991.
[226] Wang H, Wang H, Li Y, *et al*. Assessment of image quality of coronary computed tomography angiography in obese patients by comparing deep learning image reconstruction with adaptive statistical iterative reconstruction veo. *J Comput Assist Tomogr* 2022; 6:

34–40.
[227] Silberstein J, Wee C, Gupta A, *et al*. Artificial intelligence-assisted detection of osteoporotic vertebral fractures on lateral chest radiographs in post-menopausal women. *J Clin Med* 2023; 12: 7730.
[228] Chu M, Wu P, Li G, Yang W, Gutierrez-Chico JL, Tu S. Advances in diagnosis, therapy and prognosis of coronary artery disease powered by deep learning algorithms. *JACC Asia* 2023; 3: 1–14.
[229] Zhang N, Zhao X, Li J, *et al*. Machine learning based on computed tomography pulmonary angiography in evaluating pulmonary artery pressure in patients with pulmonary hypertension. *J Clin Med* 2023; 12: 1297.
[230] Sun Z, Ng CK. Finetuned super-resolution generative adversarial network (artificial intelligence) model for calcium deblooming in coronary computed tomography angiography. *J Pers Med* 2022; 12: 1354.
[231] Lin A, Manrai N, McElhinney P, *et al*. Deep learning-enabled coronary CT angiography for plaque and stenosis quantification and cardiac risk prediction: an international multicentre study. *Lancet Digit Health* 2022; 4: e256–e265.
[232] Eng D, Chute C, Khandwala N, *et al*. Automated coronary calcium scoring using deep learning with multicentre external validation. *NPJ Digit Med* 2021; 4: 88.
[233] Quer G, Arnaout R, Henne M, Arnaout R. Machine learning and the future of cardiovascular care: JACC State-of the art review. *J Am Coll Cardiol* 2021; 77: 300–313.
[234] Mu D, Bai J, Chen W, *et al*. Calcium scoring at coronary CT angiography using deep learning. *Radiology* 2022; 302: 309–316.
[235] Winkel DJ, Suryanarayana VR, Ali AM, *et al*. Deep learning for vessel-specific coronary artery calcium scoring: validation on a multi-centre dataset. *Eur Heart J Cardiovasc Imaging* 2022; 23: 846–854.
[236] Gogin N, Viti M, Nicodeme L, *et al*. Automatic coronary artery calcium scoring from unenhanced-ECG-gated CT using deep learning. *Diagn Interv Imaging* 2021; 12: 989250.
[237] Diller GP, Benesch Vidal ML, Kempny A, *et al*. A framework of deep learning networks provides expert-level accuracy for the detection and prognostication of pulmonary arterial hypertension. *Eur Heart J Cardiovasc Imaging* 2022; 23: 1447–1456.
[238] Van der Bijl P, Bax JJ. Using deep learning to diagnose pulmonary hypertension. *Eur Heart J Cardiovasc Imaging* 2022; 23: 1457–1458.
[239] Yang G, He Y, Lv Y, *et al*. Multi-task learning for pulmonary arterial hypertension prognosis prediction via memory drift and prior prompt learning on 3D chest CT. *IEEE J Biomed Inform* 2023; 27: 1967–1978.
[240] Jiang B, Guo N, Ge Y, *et al*. Development and application of artificial intelligence in cardiac imaging. *Br J Radiol* 2020; 93: 20190812.

Please cite this article as: SUN ZH. Cardiovascular computed tomography in cardiovascular disease: An overview of its applications from diagnosis to prediction. *J Geriatr Cardiol* 2024; 21(5): 550–576. DOI: 10.26599/1671-5411.2024.05.002